Role of purinergic receptor $2X_7$ in renal disease and non-alcoholic steatohepatitis (NASH) associated with metabolic disorders through activation of the NLRP3 inflammasome.

Claudia Blasetti Fantauzzi

Ph.D. program: "Molecular Medicine"

XXV Cycle

Coordinator	**Tutor**
Prof. Alberto Gulino	Prof. Giuseppe Pugliese

Index

Introduction

Preface

In the pathogenesis of chronic complications of diabetes - both micro- and macro-vascular complications -, low-grade systemic inflammation is a major contributor in the development of cell and tissue damage induced by the metabolic abnormalities that characterize the disease.

On the other hand, large portions of the human genome are dedicated to 2 functions closely related to each other: the innate immunity and the energy metabolism of the cell. From the evolutionary point of view, for most of the human history, the pressure from infection, trauma and starvation have selected individuals with more pronounced inflammatory response and gluconeogenesis capacity and, therefore, insulin resistance. However, in more recent times, due to the absence of these threats, or even for the transition to a state of oversupply, these features have produced a maladaptive response that is at the basis of the tumultuous development of metabolic and vascular diseases just mediated by the interactions between these two biological functions.

1.1 The metabolic syndrome

The metabolic syndrome (MS) is defined by a cluster of interrelated factors, such as dyslipidemia, elevation of arterial blood pressure (BP) and dysregulated glucose homeostasis (Kassi et al. 2011), that confer an increased risk for cardiovascular disease, chronic kidney disease (CKD) (Kurella et al. 2005) and non-alcoholic steatohepatitis (NASH) (Marchesini et al. 2003). Among the disorders clustering in the MS, dyslipidemia, that is elevated triglycerides and apolipoprotein B (apoB)-conteining lipoproteins, and low high-density lipoproteins (HDL), has been recognized as a powerful independent risk factor for cardiovascular disease (Castelli et al. 1986) and NASH. In the liver, insulin resistance and the MS cause fat accumulation via increased fatty acids (FA) delivery from adipose tissue and enhanced hepatic FA import and synthesis exceeding the rate of FA export and catabolism. In contrast, a causal role for dyslipidemia and MS in renal disease has been demonstrated only in studies in experimental animal models, showing that a high saturated fat and/or cholesterol intake induces glomerulosclerosis and tubulo-interstitial damage, associated with renal lipid accumulation, altered cellular lipid

metabolism and non-enzymatic lipid modifications causing lipotoxicity (Jiang et al. 2005; Kume et al. 2007; Deji et al. 2009; Iacobini et al. 2009). In addition, the increased lipid synthesis and deposition driven by the up-regulation of sterol regulatory element-binding protein-1 was shown to contribute significantly to renal injury occurring in experimental diabetes (Sun et al. 2002).

The MS is characterized by a low-grade chronic inflammation, often referred to as "metaflammation", being a metabolically triggered inflammation. In this condition, nutrients and metabolic surplus, rather than pathogens, act as principal triggers of the inflammatory response engaging the same molecules and signaling pathways as those involved in classical inflammation (Hotamisligil et al. 2006). However, although inflammation and consequent fibrosis were proposed as possible pathogenetic mechanisms linking lipotoxicity to renal and liver damage (Deji et al. 2009; Iacobini et al. 2009), to date, the molecular basis of activation of renal and liver pro-inflammatory and fibrogenic signaling pathways by an obesogenic high-fat diet (HFD) is still poorly defined.

1.2 Innate immunity

The inflammatory response mediated by the innate immune system plays an important role in host safeguard and it is one of the first lines of defense to be activated by pathogens. In the case of microbial invasion, it often plays a critical role in clearing, containing, and/or slowing the infection.

Innate immunity is characterized by its ability to recognize a wide range of pathogens such as viruses, bacteria, fungi and parasites by a limited number of germline-encoded receptors called pattern-recognition receptors (PRRs). PRRs are able to recognize several well-conserved microbial structures, which are known as pathogen-associated molecular patterns (PAMPs), triggering proinflammatory signaling. Examples of PAMPs are sugars, flagellin, and the cell wall components peptidoglycan (PGN) and lipopolysaccharide (LPS). It is now clear, however, that the innate immune system can also respond to non-microbial stimuli. Interestingly, accumulating evidence reveals that some of PRRs are also able to sense various endogenous signals that arise during tissue or cell damage, termed damage-associated molecular patterns (DAMPs), as well as particulate exogenous non-

microbial compounds, like asbestos fibers or silica. During infection, DAMPs provides additive signals to those induced by PAMPs. However, DAMP signaling can also trigger inappropriate inflammation in sterile types of injury and thereby contribute to unnecessary organ damage and dysfunction (Anders and Muruve 2011). Both infectious and sterile stimuli ultimately lead to the same downstream vascular and cellular manifestations of inflammation (*Figure 1*).

PRRs can be found both in immune cells, like macrophages, monocytes, dendritic cells (DCs), neutrophils, and non-immune cells, i.e. epithelial cells. At least five distinct genetic and functional clades of PRRs are known: Toll-like receptors (TLRs), the receptor for advanced glyco- and lipoxidation end-products (RAGE), C-type lectin receptors (CLRs), retinoic acid–inducible gene (RIG)-I-like receptors (RLRs), and the nucleotide-binding domain, leucine-rich repeat–containing (NBD-LRR) proteins (NLRs). Some of the TLRs as well as the C- type lectin receptors are found on the cell surface; additionally, the endosomal compartment contains some TLRs that sense nucleic acids. Unlike TLRs and CLRs, RLRs and NLRs are cytosolic proteins that survey for the presence of intracellular microbial molecules or danger signals.

Most of the PRRs triggers nuclear factor (NF) -kB, IFN regulatory factors, and mitogen-activated protein kinase signaling pathways resulting in the transcription of proinflammatory chemokines and cytokines or proteins involved in antigen presentation and processing. In the last years, however, a prominent subgroup of NLRs involved in the post-translational activation of pro-inflammatory cytokines such as interleukin (IL)-1β and IL18 has been identified. The generation of mature IL-1β and IL-18, indeed, involves two separate processes to avoid their inappropriate and deleterious release: the induction of NF-kB-dependent mRNA expression and translation of the procytokine upon activation by most PRRs (signal 1) followed by cleavage of the procytokine and release of its mature and active form (signal 2). The latter event depends on the assembly and activation, in response to an appropriate microbial and non-microbial stimulus, of multiprotein complexes termed ‘inflammasomes’ that mediate caspase-1-dependent processing of the procytokines (Anders et al. 2001; Bauernfeind et al. 2011) (*Figure 1*).

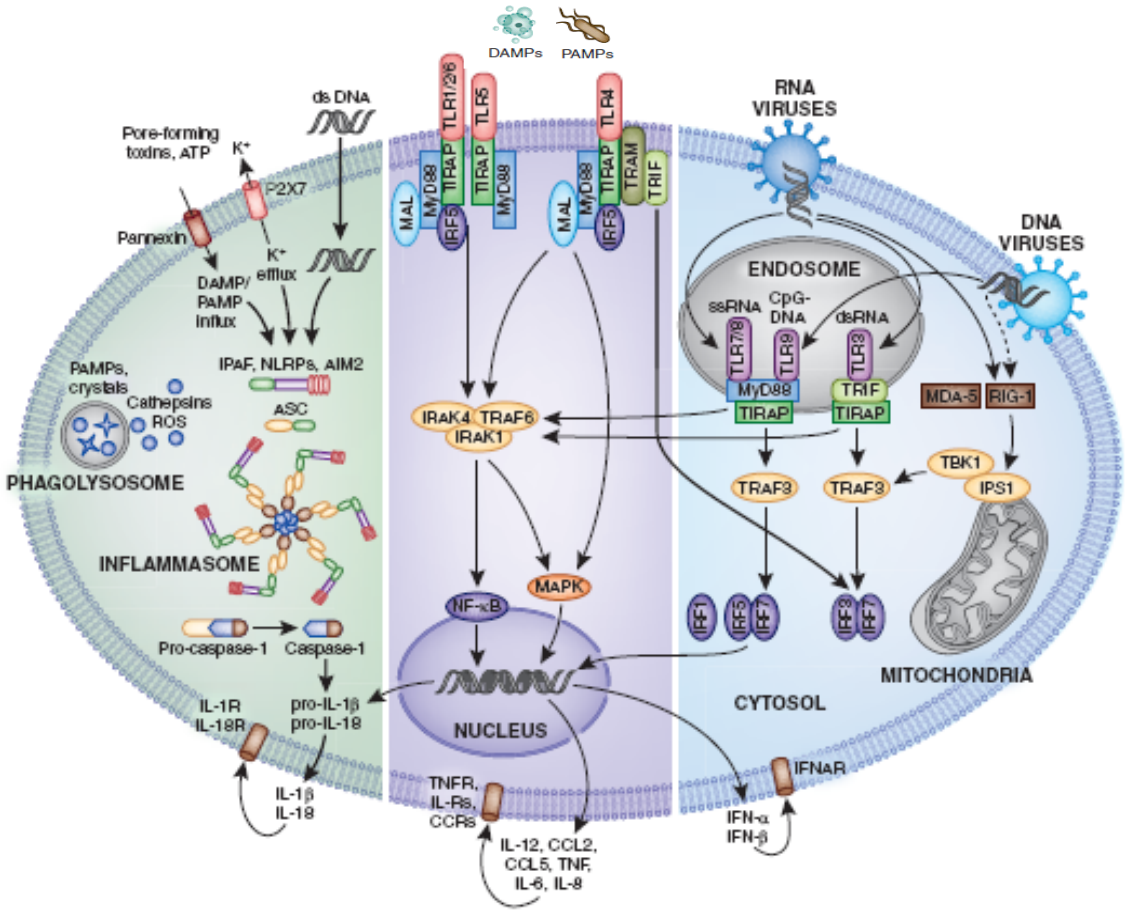

Figure 1. How pattern recognition receptors induce innate immunity. Several groups of extracellular or intracellular innate pattern recognition receptors exist. TLR-1/2/4/5/6 recognize microbes at the cell surface. TLR3/7/8/9 recognize viral and bacterial nucleic acids in intracellular endosomes. All TLRs use the intracellular adaptor myeloid differentiation primary response gene (88) (MyD88) for downstream signaling, except for TLR3, which uses TIR-domain-containing adapter-inducing interferon-β (TRIF). TLR4 uses MyD88 and TRIF. All TLRs can induce the expression of NF-kB-dependent genes, including most proinflammatory cytokines and chemokines. TLRs also induce the procytokines IL-1β and IL-18 (signal 1). These cytokines need caspase-1 activation as a second step before they can be released. Caspase-1 activation is under the control of the inflammasomes. For example, potassium efflux, lysosomal cathepsin leakage in the cytosol, or oxidative stress can trigger the NLRP3 inflammasome that includes the adaptor ASC and caspase 1. All cytokine classes amplify innate immunity by interacting with their respective cytokine receptors, as shown at the bottom of the figure. All inflammasome-related cytokines ligate their receptors to trigger MyD88-dependent signaling. (*Anders and Muruve 2011*)

1.3 Inflammasomes

Some NLRs have recently been identified as component of the inflammasome complex, a multiprotein oligomer whose assembly leads to caspase-1 activation. Specifically, the inflammasome's NLR component is able to sense the pro-inflammatory stimuli, inducing in turn the platform assembly.

NLRs display a tripartite structural organization consisting of (Bauernfeind et al. 2011)

- *C-terminal leucine-rich repeats* (LRRs), suited for ligand binding, although a clear receptor-ligand interaction has not been demonstrated for any NLR yet;
- *a central NBD or NACHT domain* (nucleotide-binding domains or NAIP, CIITA, HET-E, and TP-1) that is thought to oligomerize upon activation in the presence of ATP;
- *an N-terminal effector domain* necessary for signal transduction through protein–protein interactions. Based on the molecular structure of the N-terminal domain (Ting et al. 2008), different NLR subfamilies can be distinguished. For the purpose of the work we refer only to the two major subfamilies: the NLRCs, to which also belong NODs (NOD-like receptor family), containing a *caspase recruitment* domain (CARD) and the NLRPs, which instead contain a *pyrin* domain (PYD). CARD and PYD domains are able to interact only with subunits of identical chemical nature, CARD with CARD and PYD with PYD. (*Figure 2*).

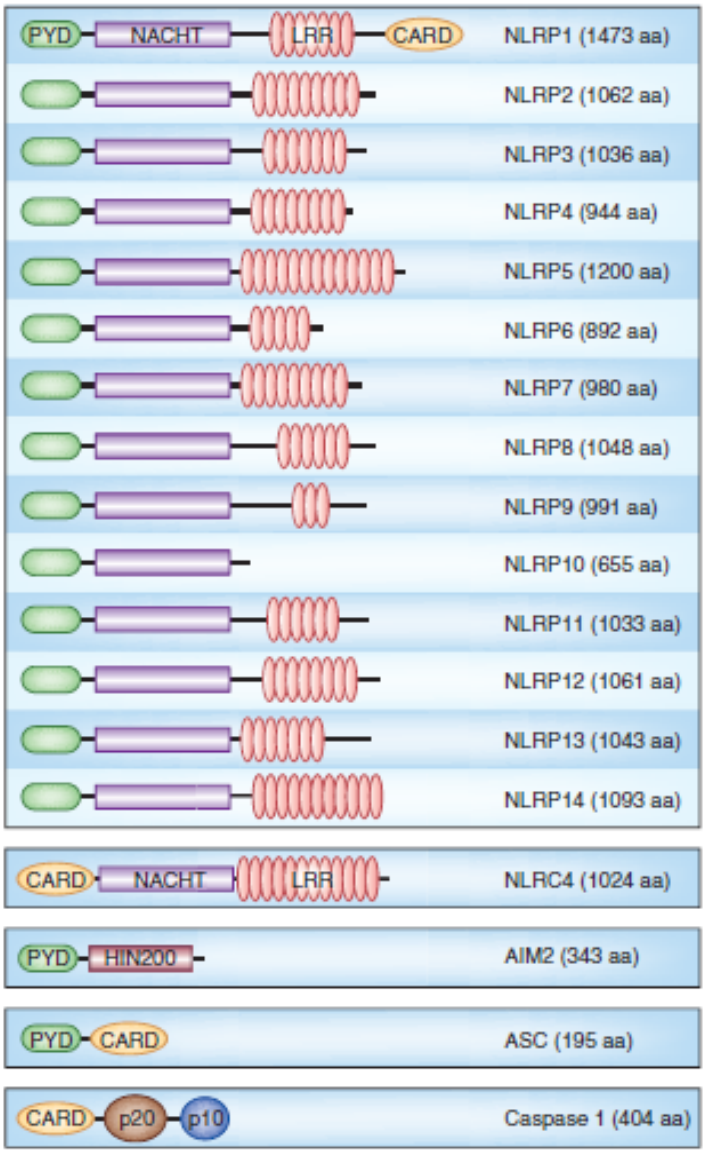

Figure 2. Human inflammasome-related genes. The NLRP subfamily of NLR genes consists of 14 members that are typified by an N-terminal PYD in addition to conserved NACHT and leucine-rich repeat domains common to all NLR genes. NLRP1 is unique in that it also carries a C-terminal CARD. NLRC4 (Ipaf1) is a member of the NLR family with an N-terminal CARD that can directly interact with caspase-1. AIM2 is a DNA interacting human interferon-inducible 200 protein with an N-terminal PYD that can form a caspase1-activating inflammasome but does not belong to the NLR family. Inflammasomes also generally consist of the adaptor protein ASC and the cystine protease caspase-1 (*Anders and Muruve 2011*).

Exposure to a specific DAMP or PAMP leads to the oligomerization of some NLRs via their NACHT domain and the consequent recruitment of the adapter protein ASC (apoptosis-associated speck-like protein containing a CARD) via direct interaction PYD-PYD. ASC, in turn, recruits procaspase1 via a homotypic CARD interaction to complete the formation of inflammasome. Recruitment to the inflammasome triggers procaspase-1 autoprocessing and generation of the active forms 10 kDa (p10) and 20 kDa (p20) that associate into enzymatically active p10/20 heterodimers. In turn, active caspase-1 cleaves the 31 kDa pro-IL-1β and the 22 kDa pro-IL-18 into their active and secreted forms (17 kDa and 18 kDa respectively) (Anders et al. 2011) *(Figure 3)*.

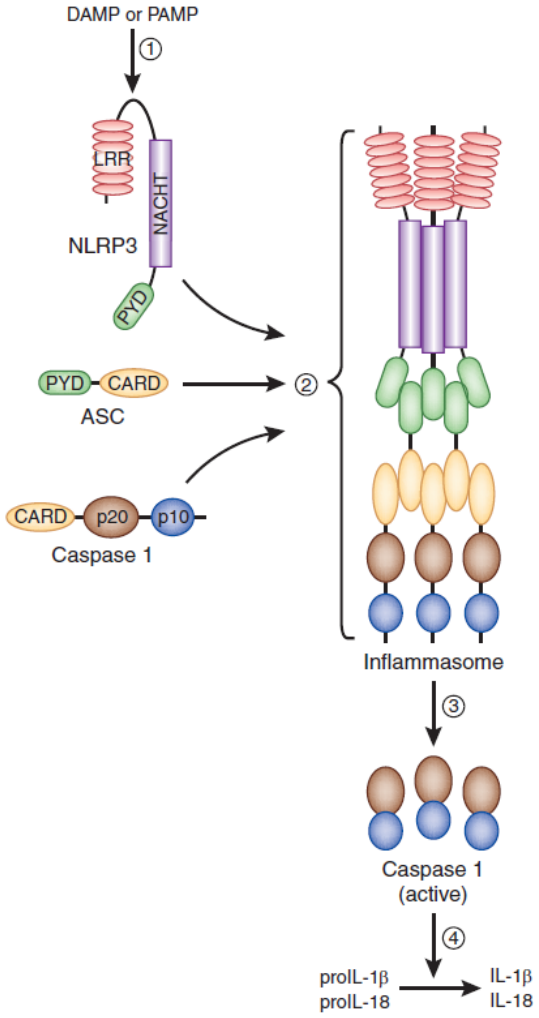

Figure 3. Simplified model of NLRP3 structure and activation. (1) Exposure to a DAMP or PAMP releases NLRP3, which oligomerizes via its NACHT domain. (2) NLRP3 oligomerization recruits the adapter protein ASC to the complex. ASC then recruits caspase-1 via a homotypic CARD interaction to complete the formation of the inflammasome.(3) Recruitment to the inflammasome triggers caspase-1 autoprocessing and generation of the active p10/20 heterodimeric enzyme. (4) Active caspase-1 cleaves pro-IL-1β and pro-IL-18 into their active and secreted forms (*Anders and Muruve 2001*).

Caspase 1 is the best described inflammatory caspase, so termed because the precursor forms of the inflammatory cytokines IL-1β and IL-18 are its main substrates (Martinon et al. 2009). Under certain conditions, activation of caspase 1 leads to a particular type of programmed cell death termed "pyroptosis", that, in contrast to the silent apoptosis, is associated with a high inflammatory state. Pyroptosis is initiated by a variety of stimuli, including cytosolic flagellin, phagocytosis of crystals and opening of pores in the membrane and, as oncosis/necrosis, it results in the lysis of the cell and release of cytosolic contents (Miao et al. 2011; Majno and Joris 1995).

Four inflammasome complexes have been partially characterized to date. While NLRP1 and NLRC4 seem to recognize only specific bacterial components, so being involved only in the inflammatory sepsis cascade, the AIM2 and NLRP3 inflammasomes assemble also in response to endogenous signals, thus playing a role also in sterile inflammation (Bauernfeind et al. 2011).

To date, the **NLRP3** inflammasome is by far the best-characterized one and its dysregulation has been associated with many disorders, including kidney and liver diseases.

1.3.1 The NLRP3 inflammasome

The NLRP3 inflammasome, also known as cryopirin or NALP3, is composed by the sensor NLRP3, the adapter protein ASC and the protease caspase1 (*Figure 3*).

NLRP3 is expressed primarily in macrophages and dendritic cells (Schroder and Tschopp 2010), but also in cells of non-hematopoietic tissues, including epithelial cells and osteoblasts (McCall et al. 2008).

A role for NLRP3 inflammasome in recurrent and chronic inflammation was initially described in a group of rare autoinflammatory conditions, termed cryopyrin-associated periodic syndrome (CAPS), characterized by NLRP3/CIASI mutations that cause spontaneous activation of the NLRP3 inflammasome complex leading to excessive IL-1β secretion (Agostini et al 2004) and associated sterile inflammation. Subsequently, inflammasomes have been implicated in the pathology of many common diseases, including cancer, gout and diabetes (Cook et al. 2010).

The initial priming step (signal 1), required for subsequent NLRP3 inflammasome activation, can be mediated by various PRRs-ligands (both PAMPS and DAMPs) and inflammatory cytokines, including LPS, CpG, and TNF-α (Guarda et al. 2011). Priming induces activation of NF-kB and is crucial not only to produce a pool of pro-IL-1β substrate, but also to boost NLRP3 expression to a functional level (Bauernfeind et al. 2009, Franchi et al. 2009).

Several microbial and non-microbial stimuli, associated with both infectious and non-infectious diseases, are known to trigger NLRP3 inflammasome activation acting as signal 2. The microbial stimuli include cell wall component and toxin derived from bacteria and fungi. In addition, the NLRP3 inflammasome is able to sense viral RNA and adenoviral DNA, thus playing a role in the control of viral infections (Zambetti et al. 2012).

Non-microbial activators include both particulate exogenous compounds, like asbestos fibers or silica, that provoke inflammatory disorders such as silicosis and asbestosis, and many DAMPs produced by host damaged cells and associated with several diseases. For example, in pathological conditions, injured or necrotic cells release high levels of adenosine triphosphate (ATP) that acts as danger signal. Moreover, the causative agent of osteoarthritis, i.e., the basic calcium phosphate crystals, seems to play a role in NLRP3 inflammasome activation and IL-1β secretion (Martinon et al. 2006). Likewise, fibrillar amyloid-β, involved in the pathogenesis of Alzheimer's disease, as well as serum amyloid A (SAA), a crucial acute-phase protein in amyloid A-type amyloidosis, are both able to activate caspase 1 via NLRP3 inflammasome (Niemi et al. 2011, Salminen et al. 2008). Even the adjuvant properties of aluminum hydroxide (alum) have been shown to depend on activation of the NLRP3 inflammasome (Eisenbarth et al. 2008).

Moreover, recent papers have reported a crucial role for the NLRP3 inflammasome in several metabolic diseases, such as gout, atherosclerosis, type 2 diabetes (T2D) and obesity (De Nardo and Latz 2011).

Gout, historically known as a 'disease of kings' as it is thought to result from a diet rich in purines, is a chronic inflammatory condition related to the deposition in the joints of uric acid crystals or monosodium urate, MSU. These compounds act as NLRP3 inflammasome danger signals causing the release of IL-1β and the inflammatory responses in joints (Martinon et al. 2006).

Likewise, atherosclerosis is a chronic inflammatory disease characterized by the accumulation of lipid components, particularly low density lipoproteins (LDLs), within the intima of the artery wall, where they are modified (e.g. oxidized). Accumulation of modified LDLs promotes both recruitment of monocytes, with the subsequent formation of cholesterol-engorged macrophage foam cells, and the formation of cholesterol crystals (Duewell et al. 2010, Klinkner et al. 1995). Interestingly, it has recently shown that modified LDLs function as signal 1 increasing the expression of pro- IL-1β in macrophages via a receptor complex involving various TLRs (Stewart et al. 2010) and scavenger receptors (Febbraio et al. 2000), while cholesterol crystals act as activator molecules of the NLRP3 inflammasome (Duewell et al. 2010).

Moreover, a role for the NLRP3 inflammasome in the T2D onset and progression has been proposed, since IL-1β promotes beta-cell dysfunction and cell death directly (Mandrup-Poulsen et al. 2010). It was demonstrated that the islet amyloid polypeptide (IAPP or amylin), a hormone secreted together with insulin, is deposited in the islet interstitium of patients with type 2 diabetes and forms amyloid structures able to activate the inflammasome (Westermark et al. 2011, Masters et al. 2010). Other studies have also suggested that high glucose concentrations induce β-cell production and release of IL-1β *in vitro*, which in turn promotes functional impairment and apoptosis of the β-cells in an autocrine manner (Maedler et al. 2002). Furthermore, several evidences link insulin homeostasis to NLRP3 inflammasome activation, since glyburide, a widely used therapeutic insulin secretagogue, can inhibit NLRP3 inflammasome–mediated caspase-1 activation and the release of both IL-18 and IL-1β (Lamkanfi et al. 2009). Moreover, mice knock out for any of the constituents of the NLRP3 inflammasome fed a high-fat diet (HFD), show improved glucose tolerance and insulin sensitivity, linking the NLRP3 inflammasome to insulin resistance (Wen et al. 2011, Stienstra et al. 2011, Zhou et al. 2010, Stienstra et al. 2010, Vandanmagsar et al. 2010).

It has long been postulated that obesity is a strong risk factor for insulin resistance and type 2 diabetes (Hotamisligil 2006). Notably, recent studies have found that obesity itself induces the assembly of the NLRP3 inflammasome in adipose tissue macrophages, mediating insulin resistance in early T2D (Vandanmagsar et al 2010, Stienstra et al. 2010). Several endogenous danger signals have been implicated in NLRP3 activation during obesity, including the lipotoxic ceramide and the saturated

fatty acid palmitate, whose circulating levels of both are strongly increased in obesity (Wen et al. 2011, Vandanmagsar et al. 2011).

1.3.2 Models for NLRP3 inflammasome activation

As NLRP3 inflammasome can be activated by a broad range of microbial and non-microbial compounds, it seems unlikely that such different molecular structures could all interact directly with NLRP3 protein. Until now, no NLRP3 activators have been indeed shown to directly interact and activate it, suggesting that NLRP3 may sense these signals indirectly.

To date, the mechanisms upstream of NLRP3 inflammasome activation are not fully elucidated. Based on the structural and biological characteristic of the activators so far identified, three models not mutually exclusive have been proposed (*Figure 4*).

In the first model, extracellular ATP activates NLRP3 inflammasome through the engagement of the purinergic receptor $2X_7$ ($P2X_7R$). This binding triggers cellular K+ efflux inducing recruitment of the pannexin-1 membrane pore that in turn allows extracellular NLRP3 agonists to access the cytosol and activate NLRP3 (Kanneganti et al. 2007).

A second models was proposed to explain the inflammasome activation mediated by particulate compounds, including MSU, cholesterol crystal, silica, asbestos, amyloid-β, and alum. Based on this mechanism, the engulfment of these molecules by phagocytes results either in the failure of the phagocytosis, a process termed "frustrated phagocytosis", or in the rupture of the lysosome membrane within the cells, with the consequent release of the lysosomal contents in the environment or into the cells respectively. The lysosomal components, particularly the protease cathepsin B, in turn could act as activator of the inflammaome (Halle et al. 2008, Hornung et al. 2008).

Finally, the third model, considered also the unifying mechanism, is based on the evidences that all NLRP3 activators induce reactive oxygen species (ROS) generation and that ROS are able to activate NLRP3 inflammasome. Several studies, moreover, have shown that NLRP3 inflammasome activation induced by particulates, ATP, nigericin, and yeast can be abrogated by ROS scavengers, suggesting that ROS

may act upstream of NLRP3 activation (Zambetti et al. 2012). ROS mainly originate by two major processes: the oxygen metabolism in the electron transport chain within the mitochondria and the activity of cellular enzymes such as NADPH oxidases, xanthine oxidoreductases, lipoxygenases and cyclooxygenases (Dröge et al. 2002). Several enzymes displaying anti-oxidant activities, including thioredoxin (TRX), superoxide dismutases, glutathione peroxidases and catalase are involved in neutralizing ROS. Indeed, ROS are important regulators of several physiological responses, including angiongenesis, cell growth and differentiation as well as innate immune responses (Martinon 2010), but an unbalance between ROS generation and neutralization can triggers the harmful oxidative stress, common denominator of many diseases, including atherosclerosis and diabetes (Valko et al. 2007). The exact mechanism that drives ROS-mediated inflammasome activation remains debated, though, recently, Zhou and collegues have demonstrated a direct interaction between NLRP3 and TRX-interacting protein (TXNIP). Inflammasome activators, including uric acid crystals and hydrogen peroxide, induce the dissociation of TXNIP from TRX in a ROS- sensitive manner and allow it to bind and activate NLRP3 (Zhou et al. 2010). However, ROS appear to be necessary but not sufficient to mediate this process, since a number of signals which generate ROS do not activate the NLRP3 inflammasome.

Recently, a major role for ATP and purinergic signal in the NLRP3 inflammasome regulation has been proposed (Gombault et al. 2012). ATP is in fact also considered an extracellular messenger able to act both in autocrine and paracrine manner, regulating many physiological and pathological processes through the binding to purinergic receptors (Pellegatti et al. 2005). In addition to passive ATP release from necrotic cells, to date it results clear that in some cell types, such as human monocytes, ATP can be released actively by several NLRP3 activators, including MSU, silica, alum crystals, and amyloid-β protein aggregates (Riteau et al. 2012). On the other hand, ATP leakage from dying autophagic cells and from phagocytosis-associated regurgitation by macrophages appears to be important for NLRP3 inflammasome activation (Gombault et al 2012).

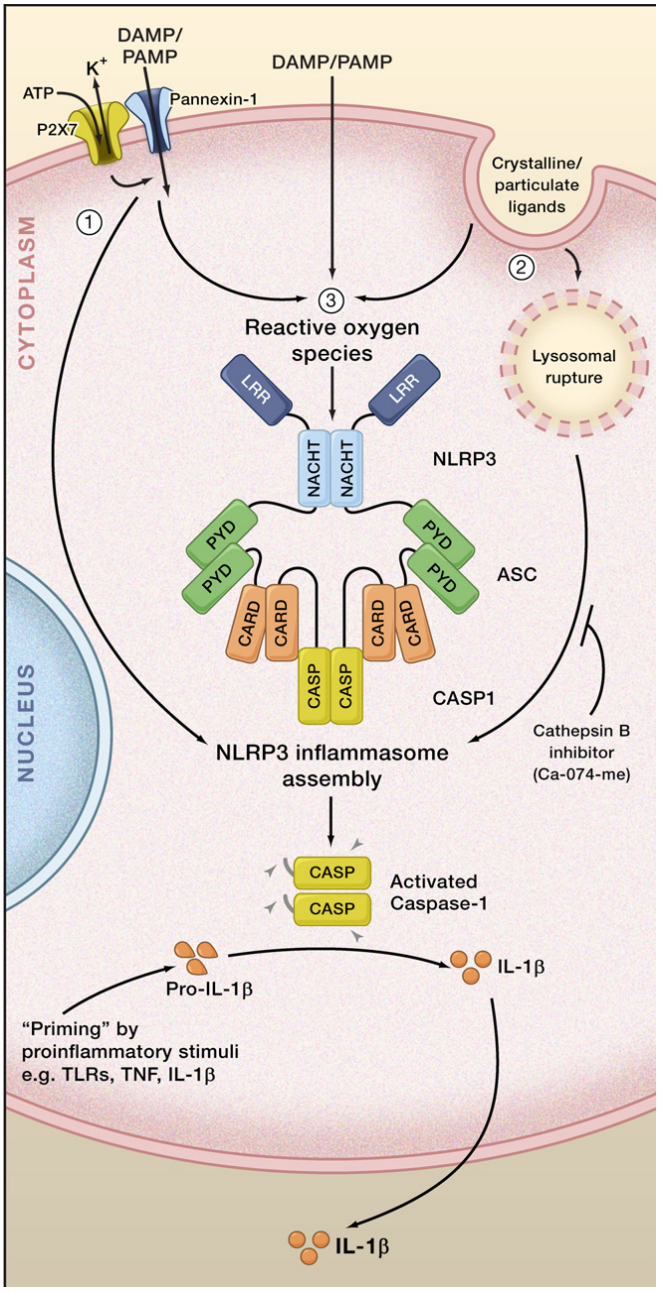

Figure 4. NLRP3 Inflammasome Activation Three major models for NLRP3 inflammasome activation are favored in the field, which may not be exclusive: (1) The NLRP3 agonist, ATP, triggers $P2X_7$-dependent pore formation by the pannexin-1 hemichannel, allowing extracellular NLRP3 agonists to enter the cytosol and directly engage NLRP3. (2) Crystalline or particulate NLRP3 agonists are engulfed, and their physical characteristics lead to lysosomal rupture. The NLRP3 inflammasome senses lysosomal content in the cytoplasm, for example, via cathepsin-B-dependent processing of a direct NLRP3 ligand. (3) All danger-associated molecular patterns (DAMPs) and pathogen-associated molecular patterns (PAMPs), including ATP and particulate/crystalline activators, trigger the generation of reactive oxygen species (ROS). A ROS-dependent pathway triggers NLRP3 inflammasome complex formation. Caspase-1 clustering induces autoactivation and caspase-1-dependent maturation and secretion of proinflammatory cytokines, such as IL-1β and IL-18 (*Schroder and Tschopp 2010*).

1.4 ATP as extracellular messenger

ATP has several features that make it an ideal extracellular messenger: the very low extracellular levels under quiescent conditions, the high cytosolic concentration, the quick release in pericellular environment caused by many different stimuli, the fast degradation in the extracellular space by enzymes expressed on the cell surface, and the presence of specific receptors (Burnstock et al. 2007).

The cytosolic concentration of ATP in mammalian cells is rather high: the cytoplasm of most neurons contains 2–5mM ATP, and higher concentrations of ATP (up to 100 mM) are stored in synaptic vesicles. Sperm, tumor cells, and the epithelial cells of the lens of the eye have exceptionally high intracellular levels of ATP and granules in adrenal chromaffin cells, Merkel cells, platelets, and pancreatic insulin-containing cells also contain significant amounts of nucleotide (Novak 2003).

ATP efflux from diverse cell types may be elicited by a variety of stimuli, including hypoxia, acidosis, mechanical deformation, hyposmotic shock, receptor stimulation, fluid shear stress, and membrane depolarization. (Beigi et al. 1999)

Responses elicited by this nucleotide range from chemotaxis to cell adhesion, cytokine release to neurotransmitter secretion, activation of apoptosis to stimulation of cell proliferation (Pellegatti et al. 2005).

1.4.1 ATP release

There are three general mechanisms by which intracellular ATP can be released to extracellular spaces.

- The first involves direct, nonspecific cytolysis of healthy cells by physical and biological traumas. In the case of cellular damage, high amounts of nucleotides are secreted and such release represents a danger signal that stimulates the inflammatory response and the repair mechanisms;
- A second mechanism involves the release of ATP compartmentalized within exocytosis-competent granules or vesicles. ATP is co-packaged in the secretory granules of many neuronal, neuroendocrine, or endocrine cells and

is rapidly released during synaptic neurotransmission and other types of regulated exocytosis;

- A third potential route for ATP release is the efflux of cytosolic ATP via plasma membrane transport proteins. (Beigi et al. 1999).

1.4.2 ATP breakdown

In the extracellular space, the concentration of ATP is regulated by **ectoenzymes**, enzymes expressed on the cell surface whose catalytic site faces the extracellular milieu, such as:

- ectonucleoside triphosphate diphosphohydrolases (E-NTPDasi), that degrade both ATP and adenosine diphosphate (ADP) to adenosine monophosphate (AMP) and inorganic phosphate;
- ectonucleotidepyrophosphatases/phosphodiesterases (E-NPP), that degrade ATP to AMP and pyrophosphate;
- alkaline phosphatase, that remove phosphate groups from many types of molecules, including nucleotides.

AMP is then hydrolyzed by 5′ -nucleotidase to generate adenosine (Solini et al. 2005).

These enzymes maintain the concentration of ATP in the extracellular fluids at very low levels in the order of 5-20 μM.

Once the ATP molecule is released into the extracellular milieu, ATP, as an agonist, can bind to two subclasses of P2 purinergic receptors: the P2Y G-protein-coupled receptors and the P2X receptor channels (Schwiebert 2001).

1.5 Purinergic receptors

Purinergic receptor, or purinoceptor, are a family of receptors (P1 and P2) classified according to their molecular structure and to the relative potency of purine nucleotides and nucleosides in stimulating them.

P1 receptors are G protein-coupled receptors also known as adenosine receptors (ARs) for their ability to bind this nucleoside and are divided into four subtypes: A1R, A2AR, A2BR, and A3R (Ralevic and Burnstock 1998). Adenosine accumulates in the extracellular space in response to metabolic stress, cell damage and in conditions of ischaemia, hypoxia, inflammation and trauma (Haskó et al. 2008).

P2 receptors are activated by extracellular nucleotide and are further divided into two major families, a P2Y family of G-protein-coupled receptors (P2YR) and a P2X family of ligand-gated ion channel receptors (P2XR). The native agonist for P2XRs is ATP, whereas both ATP and its metabolite ADP act as agonists for P2YRs in a receptor-specific manner. Other endogenous nucleotides, such as UTP, UDP, and UDP-glucose, are potent agonists for some P2YRs, but they have no activity on P2XRs (Jacobson and Gao 2006).

1.5.1 P2X receptors

P2XRs are nonselective cation-conducting channels present in multiple species, from unicellular organisms to humans. ATP binds to and activates purinergic 2X receptors, thus causing transmembrane calcium, sodium and potassium fluxes, with consequent membrane depolarization that may drive further calcium influx (Solini et al. 2005).

Seven mammalian purinergic 2X receptor subunits, denoted $P2X_1$ through $P2X_7$, and several spliced forms of these subunits have been identified (North 2002).

The P2X subunit proteins are 379 ($P2X_6$) to 595 ($P2X_7$) amino acids long. Each isoform consists of two membrane-spanning α-helices (TM1 and TM2), the first involved with channel gating and the second lining the ion pore; a large extracellular

domain (comprising at least 50% of the total molecular mass); and intracellular N- and C-termini, possessing consensus binding motifs for protein kinases. From the amino terminus to the second transmembrane domain, the isoforms are 37–48% identical, with 10 conserved cysteine residues in the extracellular domain of each isoform. These cysteines may be important in stabilizing the ATP-binding pocket, which may involve regions of the extracellular loop adjacent to TM1 and TM2. P2XRs share a similar agonist binding site with some variations in the binding pocket or gating, which account for receptor specificity in agonist and antagonist binding/receptor gating. Eight residues have the potential to contribute to the formation of the ATP binding site: Lys67, Lys69, Phe185, Thr186, Asn293, Phe294, Arg295, and Lys313 ($P2X_4R$ numbering). Positively charged lysines seem to coordinate the binding of the negatively charged phosphate tail of ATP, whereas aromatic phenylalanine residues could coordinate the binding of the ATP adenine ring directly or indirectly (Surprenant and North 2009).

The carboxyl terminus of each of the isoforms is the most variable (Burnstock 2007, Schwiebert 2001).

P2X receptor subunits can combine to form either homomultimers or heteromultimers. Heteromultimers are clearly established for $P2X_2/_3$ receptors in nodose ganglia, $P2X_4/_6$ receptors in CNS neurons, $P2X_1/_5$ receptors in some blood vessels, and $P2X_2/_6$ receptors in the brain stem. $P2X_7$ receptors do not form heteromultimers, and $P2X_6$ receptors will not form a functional homomultimer without extensive glycosylation. $P2X_5$ receptors will assemble with any others, except $P2X_7$. The conserved cysteines in the extracellular domain play also a critical role in multimeric association of P2X receptor subunits, conferring a complex three-dimensional structure (Burnstock 2007, Schwiebert 2001).

All the P2X receptor subunits have multiple consensus sequences for N-linked glycosylation in the extracellular domain (Asn-X-Ser/Thr) considered essential for the membrane localization of the subunits. Receptors in which any two of the three sites are glycosylated, indeed, appear at the cell surface and are fully functional. Receptors in which only one site is glycosylated give barely detectable currents in response to ATP, and channels with no sites glycosylated give no current. These double and triple mutant receptors are retained within the cell (North 2002).

P2X receptors are abundantly distributed, and functional responses are seen in neurons, glia, epithelia, endothelia, bone, muscle, and hemopoietic tissues. On smooth muscles, P2X receptors respond to ATP released from sympathetic motor nerves. On sensory nerves, they are involved in the initiation of afferent signals in several viscera (e.g., bladder, intestine) and play a key role in sensing tissue-damaging and inflammatory stimuli. In the last case, $P2X_7$ receptor activation stimulates cytokine release by engaging intracellular signaling pathways (North 2002).

1.6 $P2X_7$ receptor

The $P2X_7R$ subunit, initially cloned from a rat brain cDNA library, shares an overall membrane topology with the other members of this family of receptors, consisting of two transmembrane domains connected by a large extracellular loop. The extracellular loop contains conserved cysteine, lysine, and glycine residues along with a number of potential N-linked glycosylation sites, all of which contribute to the structural constraints required for ATP binding (Jiang et al. 2000, Surprenant et al. 1996). The receptor is distinguished structurally from other members of P2XRs by its long intracellular C terminus tail (240 amino acids, 120 amino acids longer than any of the other P2X members) containing multiple protein and lipid interaction motifs and a cysteine-rich 18 amino acid segment (Coddou et al. 2011). Denlinger and coworkers, indeed, have identified several sites homologous to those known to be involved in the binding of LPS, TNF and SH3 domain (Denlinger et al. 2001). This long C-terminal domain appears to modulate the function of the $P2X_7R$, because the removal of this region blunts the receptor's response to ATP. Moreover, the region from residues 551 to 581 participate in regulating the surface expression of the $P2X_7R$ (*Figure 5*).

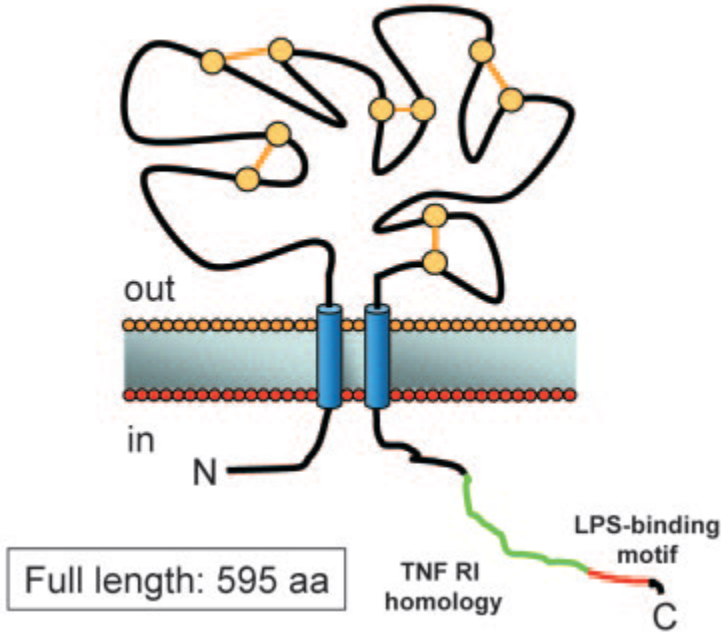

Figure 5.The $P2X_7R$: membrane topology. TNF RI homology domain (green) and putative LPS binding region (red) are shown. Cysteine residues forming putative disulfide bridges are also shown (*Adapted from Ferrari et al. 2006*).

Although originally thought to be predominately expressed on cells of hemopoietic lineages, it is emerging that the $P2X_7$ receptor has a ubiquitous distribution (Burnstock and Knight 2004), despite that, its expression levels may vary over orders of magnitude. $P2X_7R$ is present in greatest amounts on macrophages followed by dendritic cells, monocytes, natural killer cells, lymphocytes and erythrocytes in descending order (Gu et al. 2004, Gu et al. 2000). $P2X_7R$ is also present on mast cells, eosinophils, osteoclasts and microglia, while neutrophils showed no surface expression of $P2X_7$ receptors but do contain intracellular receptors (Gu et al. 2000). Finally, $P2X_7$ is also expressed on cells of non-hematopoietic origin including bone cells, epithelial cells from the skin, kidney, reproductive and urinary tracts (Burnstock and Knight 2004), fibroblasts (Solini et al. 1999), endothelial cells (Wilson et al. 2007), exocrine glands (salivary glands and pancreas) (Novak 2008) as

well as glomerular cells, mainly podocytes but, to a lesser degree, also endothelial and mesangial cells (Vonend et al. 2004).

$P2X_7R$ is the least sensitive member of the P2XR family to activation by nucleotides. It is activated by extracellular *ATP* (EC50 > 80 – 100 μM) and the more potent ATP analogue, 2′ ,3′ -(benzoyl-4-benzoyl)- ATP, (*BzATP*) (EC50 = 7 μM) (Surprenant et al. 1996). Other analogues like *2-meSATP* and *ATPγS* are partial agonists of this receptor, whereas *αβ-meATP* and *βγ-meATP* have very little effect on activation. These analogs are metabolically more stable than ATP being relatively resistant to breakdown by ectonucleotidases. A few years ago, Kim and collegues (Kim et al. 2001) showed that the $P2X_7$ receptor becomes dephosphorylated on Tyr-343 as a result of exposure to agonist. The direct demonstration that the $P2X_7$ receptor complex in HEK293 cells contains a receptor protein tyrosine phosphatase (RPTP β) favors the interpretation that this is activated when ATP binds to the receptor and exert a feedback control of the channel itself through its dephosphorylation.

Several compounds act as P2XR antagonists. The first functional studies of P2X receptors were based on the evidence from the broad inhibitory effects of suramin, an agent introduced almost a century ago for the treatment of trypanosomiasis, of 2′ ,3′ -dialdehyde ATP (*oxidized ATP*), and pyridoxalphosphate-6- azopheny-2′ ,4′ -disulfonate (*PPADS*). However, these compounds are not specific for $P2X_7R$ (Hibell et al. 2001, Surprenant et al. 1996). The first relatively specific $P2X_7R$ antagonist identified was *KN-62*; however, it blocks currents in cells expressing the human $P2X_7$ receptor but has little effect on the rat $P2X_7R$ (Humphreys et al. 1998) and at high concentrations it also blocks Ca^{2+} /calmodulin-dependent protein kinase II. Selective antagonists of $P2X_7R$ activation have only recently become available. Two of these antagonists, *A-438079* and *A-740003*, have been shown to impair nociception in rodent models of neuropathic and inflammatory pain (Donnelly-Roberts and Jarvis 2007). These *in vivo* findings support therapeutic trials of $P2X_7R$ blockers, and at least two $P2X_7R$ antagonists, *CE-224535* (Pfizer) and *EVT 401* (Evotec), are currently undergoing various phase I or II trials. In addition to chemical antagonists, the *anti-human $P2X_7R$ mAb* (clone L4) can impair human $P2X_7R$ function including $P2X_7R$-induced cation fluxes and IL-1β release (Buell et al. 1998).

$P2X_7R$ activation is also inhibited by many divalent cations with a rank potency of $\underline{Cu^{2+} > Cd^{2+} = Zn^{2+} > Ni^{2+} >> Mg^{2+} = Co^{2+} > Mn^{2+} > Ca^{2+} = Ba^{2+} >> Sr^{2+}}$ (North 2002). Some of the divalent cations may function by altering the affinity of ATP binding to $P2X_7R$ (Jiang 2009) (acting as allosteric modulators) or by making complexes with ATP, reducing the free acid form of ATP (or ATP^{4-}) in solution.

Agonist binding to the $P2X_7$ receptor opens a non-selective cation channel permeable to both monovalent (Na^+, K^+) and divalent (Ca^{2+}, Sr^{2+}, Ba^{2+}) cations causing plasma membrane depolarization. The intrinsic ion channel opens rapidly within milliseconds of agonist binding, and there is little or no rectification nor desensitisation of inward currents as measured by electrophysiology (North 2002, Surprenant et al. 1996).

One of the most defining and peculiar characteristics of $P2X_7R$, which follows activation of the receptor when the agonist application is prolonged or repetitive, is the slow development over tens of seconds of a secondary permeability pathway or 'pore' that permits the entry into cells of large organic molecules up to 900 Da and the leakage of metabolites (a process known as cell "permeabilization"). This pore pathway can be measured using or propidium dyes such as ethidium$^+$ (314 Da) or YO-PRO-1^{2+} (375 Da), that become fluorescent when they intercalate nucleic acids, giving a direct measure of their entry into cells (Wiley et al. 2011).

A key question that is raised is whether these two properties, i.e., the opening of a selective cation channel and the later formation of non-selective pores, are intrinsic to the $P2X_7$ receptor protein or whether they require additional molecules to be provided by the host cell.

At least two conflicting hypotheses have been postulated to reconcile these findings (Yan et al. 2010):

(1) the pore-dilation hypothesis suggests that there is a progressive dilation of the cation-conducting pore from initially 7Å up to 40Å;

(2) the two-pore hypothesis implies the activation of an endogenous $P2X_7R$ pore permeable for inorganic cations, accompanied by sustained activation of a distinct channel permeable to larger organic cations and fluorescent dyes.

The finding that the $P2X_7R$-dependent fluorescent dye uptake correlates with recruitment of pannexin-1 hemichannels (Pelegrin and Surprenant 2006) or a

modulation of the multidrug transporter P-glycoprotein (Elliott et al. 2005) support the second hypothesis. On the other hand, Yan and collegues have recently shown that naive rP2X$_7$R activates and deactivates biphasically at higher agonist concentrations, and the slow secondary growth of current coincides with pore dilation. The generation of biphasic currents is not blocked by inhibition of pannexin-1 channels and is also observed in cells not expressing pannexins (Yan et al. 2008). Conversely, this response is abolished by the application of a P2X$_7$R-specific antagonist (Yan et al. 2010), supporting the pore-dilation hypothesis.

In 1996 Surprenant and colleagues (Surprenant et al. 1996) demonstrated the importance of the C-terminal tail in the formation of the pore membrane. Indeed, the truncated form of the receptor to residue 418 (P2XΔC) is unable to make the transition channel-pore. Experiments conducted with truncated P2X$_7$ receptors expressed in HEK293 and in oocytes of *Xenopus* have demonstrated the importance of at least 582 amino acids for the activation of the pore, otherwise, the channel formation occurs even if the receptor is truncated at position 380. Thus, unlike the pore, the formation of the channel requires a small portion of the intracytoplasmic tail (Smart et al. 2003). It is therefore clear that further analysis will be needed to clarify the mechanism of channel-pore transition.

1.6.1 P2X$_7$R and kidney and liver disease

Recent studies using P2X$_7$R$^{-/-}$ mice and specific receptor antagonists have associated P2X$_7$R with the onset and development of several disorders, including renal, neurological, rheumatological and respiratory diseases.

Regarding the kidney, previous studies have shown the functional differentiation of P2XRs and P2YRs in the modulation of mesangial cell and extracellular matrix (ECM) turnover. The P2XRs, especially P2X$_7$R and P2X$_4$R, were found to promote mesangial cell apoptosis (Solini et al. 2007, Harada et al. 2000) and favor glucose-induced ECM synthesis (Solini et al. 2005), whereas the P2YRs, likely P2Y$_2$R and P2Y$_4$R, were shown to induce mesangial cell proliferation (Harada et al. 2000) and to inhibit matrix production (Solini et al. 2005).

Furthermore, P2X$_7$R was found to be up-regulated in glomeruli of diabetic and

hypertensive rats (Vonend et al. 2004) and, more recently, it has been implicated in two experimental models of inflammatory renal injury, i.e. unilateral ureteral obstruction (UUO) (Gonçalves et al. 2006) and antibody-mediated glomerulonephritis (Taylor et al. 2009). Gonclaves and coworkers demonstrated that the tubulo-interstitial damage and subsequent fibrosis associated with UUO were attenuated in $P2X_7R^{-/-}$ mice, suggesting a role for tubular $P2X_7R$ in renal inflammation and fibrosis. Moreover, Taylor et al. provided strong evidence for a pathogenic role of $P2X_7R$ in a rodent model of experimental glomerulonephritis (GN) and demonstrated that $P2X_7R^{-/-}$ mice were significantly protected from antibody-mediated GN (Taylor et al. 2009, Turner et al. 2007).

Although $P2X_7R$ was found to be up-regulated in glomeruli of diabetic and hypertensive rats (Vonend et al. 2004), there is no *in vivo* evidence for the involvement of the $P2X_7R$ in the onset and progression of chronic kidney disease (CKD) associated to metabolic disorders. However, it has been shown that both glucose and free fatty acids (FFAs) rapidly up-regulate $P2X_7R$ in human islets (Glass et al. 2009), thus suggesting a role for dyslipidemia in $P2X_7R$ modulation.

Less clear is the involvement of $P2X_7R$ in the pathophysiology of liver diseases. However, recent evidence suggests that this receptor might be implicated in liver injury induced by acetaminophen (APAP) (Hoque et al. 2012). In detail, $P2X_7R^{-/-}$ mice as well as wild type mice treated with the specific $P2X_7R$ antagonist A438079 had significantly decreased APAP-induced liver necrosis and hemorrhage. Chatterjee and colleagues, moreover, suggested that in the liver $P2X_7R$ could participate in the onset of the inflammatory response to carbon tetrachloride poisoning through the activation of NADPH oxidases, thus demonstrating a $P2X_7R$ -NADPH oxidase axis in liver steatosis and fibrosis (Chatterjee et al. 2012).

1.6.2 $P2X_7R$ and innate immunity

Among P2X receptors, $P2X_7R$ is characterized by the cross-talk of its downstream signaling with the pro-inflammatory cascades (North 2002).

In response to ligand binding a variety of downstream events follows, including activation of the NF-kB, processing and secretion of pro-inflammatory IL-1β and IL-

18, microvesicle/exosome release and apoptosis of the cell (Wiley et al. 2011).

Since the cytoplasmic ATP concentration is in the millimolar range, cell injury or death mediated by both infectious and sterile stimuli cause massive ATP release into the extracellular milieu. Interacting with $P2X_7R$ expressed by resident cells, both parenchymal and immune resident cells (i.e., the reticuloendothelial system), ATP participates in the activation of pro-inflammatory signals that trigger the recruitment of circulating inflammatory cells. However, there is also compelling evidence for non-lytic ATP secretion via as yet unidentified pathways activated by host- or pathogen-derived factors (Ferrari et al. 2006).

1.6.3 $P2X_7R$ and reactive oxygen release

Nicotinamide adenine dinucleotide phosphate-oxidase (NADPH ox) is a membrane-bound enzyme complex that catalyzes the production of superoxide from oxygen and NADPH. For a long time, superoxide generation by an NADPH ox was considered a function restricted to professional phagocytes. Over the last years, six homologs of the cytochrome subunit of the phagocyte NADPH ox were found: NOX1, NOX3, NOX4, NOX5, DUOX1, and DUOX2. These enzymes share the capacity to transport electrons across the plasma membrane and to generate superoxide and other downstream reactive oxygen species (ROS). Activation mechanisms and tissue distribution of the different members of the family are markedly different. The physiological functions of NOX family enzymes include host defense, post-tranlational processing of proteins, cellular signaling, regulation of gene expression, and cell differentiation. NOX enzymes also contribute to a wide range of pathological processes. Interestingly, as mentioned above, it has recently shown that the $P2X_7$ receptor is a primary mediator of oxidative stress-induced exacerbation of inflammatory liver injury in obese mice via NADPH oxidase-dependent mechanisms (Chatterjee et al. 2012)

In the kidney, the Nox4 isoform was first identified in the early 2000s and was originally described as an oxygen sensor and regulator of kidney cell growth and because of its renal abundance was termed “renox”. However, some data point to a role for Nox4 as the major source of ROS in the kidneys during early stages of

diabetes and establish that Nox4-derived ROS mediate renal damage and inflammation/fibrosis (Gorin et al. 2005). To date, it is not known if a $P2X_7$ receptor-NADPH oxidase axis is also present in the kidney and if it plays a role in renal damage associated to MS.

1.6.4 $P2X_7R$ and NF-kB

NF-kB is a transcription factor found in almost all animal cell types and plays a key role in regulating the immune response to infection. The ATP -but not other nucleotides- binding to $P2X_7$ receptor leads to the activation of NF-kB. The subunit composition of the ATP-induced NF- kB–DNA complex is rather unusual, resulting in the sole appearance of a p65 homodimer, that is probably involved in the regulation of specific inflammatory and apoptotic target genes. This ATP-induced activation requires reactive oxygen intermediates (ROIs) and proteasome and caspase-1 proteolytic activity (Ferrari et al. 1997).

Recently, Liu and collegues have demonstrated that $P2X_7R$ is involved in the activation of NF-kB mediated by LPS and ATP, thus suggesting the involvement of this purinergic receptor in the initiation of the NF-kB-dependent inflammatory events triggered by both infections and cell damage *per se* (Liu et al. 2011).

1.6.5 $P2X_7R$ and NLRP3 inflammasome

As mentioned above, it is known that activation of the $P2X_7$ receptor has a central role in the innate immune responses through the secretion of pro-inflammatory interleukin IL-1β and IL-18 from cells of myeloid origin (Wiley et al. 2011). Early observations showed that extracellular ATP is a strong IL-1β-releasing agent (Griffiths et al. 1995, Perregaux and Gabel 1994); subsequent *in vitro* "loss of function" and "gain of function experiments", together with *in vivo* analysis conducted on $P2X_7R^{-/-}$ mice, made it possible to establish that the receptor responsible for ATP-dependent IL-1β release is the $P2X_7R$ (Solle et al. 2001, Ferrari et al. 1997, Ferrari et al. 1996). Mechanistically, the role of K^+ efflux in supporting $P2X_7R$-dependent IL-1β processing and release seems to be crucial as both processes

are suppressed by inhibition of cellular K^+ efflux (Ferrari et al. 1997, Perregaux and Gabel 1994). Consistently, mutations in the human $P2X_7R$ that impair both pore formation and ATP-stimulated K^+ efflux inhibit IL-1β and IL18 release (Sluyter et al. 2004), and several stimuli that also cause a rapid lowering of cytoplasmic K^+ , e.g. the ionophore nigericin or sucrose medium, induce robust IL1β processing. (Kahlenberg and Dubyak 2004, Sanz and Di Virgilio 2000, Ferrari et al. 1997). In addition to K^+ efflux from the cell, after $P2X_7R$ activation there is an influx of Ca^{2+}, which is also required for the release of active IL-1β (Ferrari et al. 2006, MacKenzie et al. 2001).

Also based on the evidence that cellular K^+ efflux and increased intracellular Ca^{2+} concentration are crucial for NLRP3 activation, a mechanistic link between $P2X_7R$ and NLRP3 activity in the regulation of cytokines release was suggested (Mariathasan et al. 2006). In detail, it was shown that eATP activates the NLRP3 inflammasomes through $P2X_7R$ (Bours et al. 2011), and that $P2X_7R$ -dependent IL-1β secretion requires assembly of a fully functional inflammasome since mice deficient in the adaptor protein ASC fail to process pro-IL-1β in response to ATP (Qu et al. 2007, Mariathasan et al. 2006). Therefore, in response to ATP binding, the $P2X_7$ receptor would induce inflammasome assembly and caspase 1 activation (Martinon 2008). However, the observation that LPS-primed macrophages from transgenic mice lacking $P2X_7$ receptors are unable to release IL-1β, but retain the ability to increase the synthesis of pro-IL-1β and caspase-1 in response to ATP- that is an NF-kB-dependent response (Labasi et al. 2002 , Solle et al. 2001)-suggest that $P2X_7R$ is essential for NLRP3 activation but is dispensable for NLRP3 priming. However, it is currently debated whether also extracellular ATP needs a priming signal or if it is a sufficient stimulus to induce both synthesis and activation of the NLRP3 inflammasome complex.

Furthermore, Pelegrin and Surprenant showed that signalling through pannexin-1 is required for processing of caspase-1 and releasing of mature IL-1β induced by $P2X_7$ receptor activation (Pelegrin and Surprenant 2006). The same group have proposed a model for the $P2X_7R$-mediated NLRP3 activation by which pannexin-1-pore formation, resulting from prolonged activation of $P2X_7R$, allows entry of bacterial products (PAMPs), DAMPs and extracellular ATP into the cell, which

directly activate inflammasome (Pelegrin and Surprenant 2009). Although the structural diversity within NLRP3 agonists argues against direct interaction between NLRP3 and all of its activators, it is not possible to exclude that the $P2X_7R$-mediated pannexin-1-pore formation could somehow facilitate the engagement of NLRP3 by its activators.

Aim

The innate immune system is involved in the pathogenesis of metabolic disorders, since it is now well-known that a state of low-grade chronic inflammation characterizes central obesity and plays a pivotal role in the development of the metabolic syndrome (MS) and type 2 diabetes, as well as in the complications of these disorders, including kidney and liver disease. However, to date, the molecular basis of activation of renal and liver pro-inflammatory and fibrogenic signaling pathways involved in this condition is still poorly defined.

The $P2X_7$ receptor is a purinergic receptor whose pro-inflammatory role is well established. Upon activation by its ligand ATP, several downstream events follow, including secretion of pro-inflammatory interleukins and apoptosis of the cell. Importantly, a mechanistic link between $P2X_7R$ and NLRP3 activity in the regulation of cytokines release has been recently demonstrated. However, to date, $P2X_7R$ and NLRP3 have been only associated with tissue damage induced by inflammatory diseases mediated by microbial pathogens, auto-immune diseases or models of acute injury, whereas their role in the onset and progression of complications of MS is unknown.

This study was aimed at investigating the contribution of the purinergic receptor $2X_7$ in the process driving renal/liver inflammation and injury associated with the MS and type 2 diabetes. To this end, $P2X_7R$-deficient ($P2X_7R^{-/-}$) mice were used to examine the participation of $P2X_7R$ in the development of renal and liver disease induced by an high fat diet (HFD), a well-established experimental model of diet-induced MS. Mechanistically, this study also investigated the involvement of the NLRP3 inflammasome in inflammation and tissue injury induced by the HFD and verified whether $P2X_7R$ ablation affected the NLRP3 response in this setting, in order to identify a $P2X_7R$-NLRP3 axis eventually operating in the pathogenesis of these complications of type 2 diabetes and MS. Moreover, $P2X_7R$ and NLRP3 expression analyses were also performed in kidney specimens from human subjects with type 2 diabetes.

Experimental procedures

3.1 Animal model

Adult (aged six weeks) male $P2X_7R^{-/-}$ (Glaxo strain) and wild-type (WT mice) were kindly provided by Prof. F. Di Virgilio (University of Ferrara, Ferrara, Italy). Mice were housed in a germ-free stabularium in accordance with the Principles of Laboratory Animal Care (NIH Publication No. 85-23, revised 1985) and received water and food ad libitum. The study protocol was approved by the local ethics committee. Mice from both genotypes were fed for 16 weeks with either a HFD (DIO diet D12492, 60% of total calories from fat) or a normal-fat diet (NFD, DIO diet D12450B; 10% of total calories from fat), purchased from Research Diets (Mucedola, Settimo Milanese, IT). Each group consisted of seven animals. At the end of the 16-week period, mice were placed into metabolic cages to collect urines. The next day, they were anaesthetized with intraperitoneal ketamine (Imalgene®, 60 mg/kg body weight) and xylazine (Rompum®, 7.5 mg/kg body weight) and a longitudinal incision of the abdominal wall was performed, a blood sample was obtained and both kidneys and liver were removed and weighed. Then, a sagittal section of the right kidney and a portion of liver tissue was immediately fixed by immersion in phosphate buffered 4% formaldehyde solution and processed for light microscopy examination and morphometrical evaluation. Paraffin-embedded sections were used also for immunohistochemistry. The remaining tissue from right kidney, together with left kidney and additional liver specimens, were frozen in liquid nitrogen and used for extraction of cytosolic and nuclear proteins and total RNA from renal cortex and liver tissue.

3.2 Human kidneys

Unaffected kidney samples from 6 patients with type 2 diabetes and 3 nondiabetic subjects who had undergone unilateral nephrectomy for renal cell carcinoma were used for $P2X_7R$, NLRP3 and ASC expression analysis by immunohistochemistry and RT-PCR. Samples were also evaluated for the presence and extent of renal lesions (see below).

3.3 Renal morphology/morphometry

Formalin-fixed and paraffin-embedded sections from mice and human kidneys were stained with periodic acid Shiff (PAS). Morphometrical analysis was performed by the use of a custom-made, C-language macro written with the Optimas 6.5 image analysis system (Optimas Corp, MediaCybernetics, Silver Spring, MD). The glomerular tufts considered were subsequent unselected occurrences falling in the observation field of the operator who moved the stage in a serpentine fashion from the outer cortex to the juxtamedullary region. The areas of at least 60 glomerular tuft profiles per sample were measured, the harmonic mean of the profile area (mean glomerular area, mGA) was obtained, and the mean glomerular volume (mGV) was estimated from it. Then, PAS-positive material in each of these glomeruli was quantified and expressed as percentage of the glomerular tuft area (fractional mesangial area, fMA). The color threshold was set by identifying three to five separate pixels in areas of positive staining. Finally, the mean mesangial area (mMA) was calculated by the formula: (fMA x mGA)/100. For the assessment of renal lipid accumulation, frozen mice kidney 6 μm sections were immersed in 4% formaldehyde for 1 hour, washed with distilled water and stained with oil red O (ORO) solution (Sigma, 0.5% in isopropyl alcohol-distilled water solution, 60:40) for 30 min. Finally, sections were washed, counterstained with hematoxylin, mounted and analyzed.

3.4 Liver morphology/morphometry

Liver morphology was assessed based on the American Association for the Study of Liver Disease (AASLD) Guidelines (Neuschwander-Tetri and Caldwell 2003). In hematoxylin and eosin-stained sections, steatosis grading was assessed based on the percentage of parenchyma involved (grades 0 to 3 as follows: 0, no fat; 1, <33%; 2, 33-66%; 3, >66%). Steatosis grade and the presence of inflammation (scored 0 to 3 as follows: 0, no inflammation; 1, mild; 2, moderate; 3, severe), hepatocyte degeneration (acidophil or Councilman's bodies, ballooning and Mallory's hyaline) or necrosis and fibrosis were then considered for nonalcoholic fatty liver disease

(NAFLD) classification as follows: **Class 1**: simple steatosis, predominantly microvesicular; **class 2** simple steatosis, predominantly microvesicular with scarce lobular inflammation; **class 3** micro/macrovesicular steastosis with modest lobular inflammation and ballooning degeneration; **class 4** predominantly macrovesicular steatosis, lobular and portal inflammation, balloning degeneration (either Mallory's hyaline or fibrosis). Within this system, class 3 and 4 NAFLD are similar and might be considered as a single group constituting NASH.

Subsequently, samples from NASH (i.e., class 3 and 4 NAFLD) mice was graded based on the type of fat (macrovesicular, microvesicular or mixed), and extent of inflammation (scored 0 to 3 as follows: 0, no inflammation; 1, mild; 2, moderate; 3, severe), and hepatocyte degeneration or necrosis. In detail, Grade 1, mild. Steatosis: predominantly macrovesicular, ranges from less than 33% to up to 66% of the lobules. Ballooning: occasionally observed; zone 3 hepatocytes. Lobular inflammation: scattered and mild acute (polymorphs) and chronic inflammation (mononuclear cells). Portal inflammation: none or mild. Grade 2, moderate. Steatosis: any degree, usually mixed macrovesicular and microvesicular. Ballooning: present in zone 3. Lobular inflammation: polymorphs may be noted associated with ballooned hepatocytes, and/or pericellular fibrosis; mild chronic inflammation. Portal inflammation: none, mild to moderate. Grade 3, severe (florid steatohepatitis). Steatosis: usually 66% (zone 3 or panacinar); commonly mixed steatosis. Ballooning: predominantly zone 3; marked. Lobular inflammation: scattered acute and chronic inflammation; polymorphs may appear concentrated in zone 3 areas of ballooning and perisinusoidal fibrosis. Portal inflammation: mild or moderate; not predominant or marked

Finally, sections stained with Masson's trichrome were staged for NASH by assessing the extent and distribution of fibrosis.

Stage 1: Zone 3 perivenular, perisinusoidal, or pericellular fibrosis; focal or extensive. Stage 2: As for stage 1 plus focal or extensive portal fibrosis. Stage 3: Bridging fibrosis, focal or extensive. Stage 4: Cirrhosis with or without residual perisinusoidal fibrosis.

3.5 Biochemistry and ELISA

Blood samples obtained from experimental animals were analyzed for fasting levels of glucose, cholesterol, triglycerides, aspartate and alanine transaminase by standard chemical methods (VITROS5.1 FS Chemistry System, Ortho-Clinical Diagnostics, Rochester, NY) and insulin by enzyme immunoassay (Ultrasensitive Mouse Insulin ELISA kit, Mercodia AB, Uppsala, Sweden); the homeostasis model assessment - insulin resistance (HOMA-IR) index was then calculated from fasting glucose and insulin. Serum and urine creatinine levels were assessed by HPLC. Proteinuria and albuminuria were measured using the Bradford dye-binding protein assay kit (Pierce, Rockford, IL) and the Mouse Albumin ELISA Quantitation Kit (Bethyl Laboratories, Montgomery, TX), respectively, and results were normalized by urine creatinine. The activation of NF-kB/p65 was assessed using the Mercury TransFactor NF-kB p65 kit (BD Biosciences Clontech, Palo Alto, CA) (Iacobini et al. 2009, Iacobini et al. 2005). Levels of IL-1β and IL-18 in kidneys were measured by the use of the Biochip Array Technology (Evidence®, Randox Laboratories Ltd, Crumlin, Antrim, UK).

3.6 Immunohistochemistry and Western blot analysis

Renal content and distribution of active caspase-3, fibronectin, collagen IV α1 chain, F4/80, monocyte chemoattractant protein-1 (MCP-1), the renal isoform 4 of NAD(P)H oxidase (Nox4), the advanced glycation endproducts (AGEs)/advanced lipoxidation endproducts (ALEs) Nε-(carboxymethyl)lysine (CML) and protein adducts of 4-hydroxy-2-nonenal (HNE), receptor for AGEs (RAGE), as well as renal and liver $P2X_7R$ and NLRP3 were assessed by immunohistochemistry.

Analogously to PAS positivity, the percentage of glomerular area of positive staining was calculated by means of the image analysis system Optimas™ 6.5. A region of interest was drown around the glomerulus. Then, the percentage of positive area for the specific stain (brown color) was calculated at a fixed color threshold (see above). For each kidney specimen, the average for percentage of glomerular area

from at least 60 glomeruli was used. For some antigens (F4/80 and MCP-1), positive staining was measured in 20 random fields of the renal cortex examined at a final magnification of 400X and expressed as the mean percentage of fields area occupied by the specific stain.

Renal cortex levels of caspase-1 were evaluated by Western blot analysis (Solini et al. 2007). Primary antibodies used in western blot: rabbit polyclonal antibody to caspase 1 (Millipore 06-503) and mouse monoclonal antibody to β-actin (Sigma, A5441); Secondary antibodies: Polyclonal Goat Anti-Mouse Immunoglobulins/HRP (Dako, P 0447) and Polyclonal Goat Anti-Rabbit Immunoglobulins/HRP (Dako P 0448). Bands were detected by enzymatic chemiluminescence kit (Immobilon Western, Millipore; Billerica, MA) and quantified by scanning densitometry using a GS-670 Imaging Densitometer (Bio-Rad Laboratories, Hercules, CA). Primary antibodies used in the immunohistochemistry studies.

1. rabbit polyclonal antibodies to:

- P2RX7 (Abcam, ab48871)

- NLRP3 (Sigma, HPA012878)

- active caspase-3 (Anti-ACTIVE® Caspase-3, Promega Italia, Milan, Italy);

- fibronectin (Sigma, F3648);

- collagen IV (Abcam, ab13966);

- HNE adducts (Alpha Diagnostic International, San Antonio, TX, USA);

- recombinant full length rat MCP-1 (Abcam, ab7202);

- recombinant mouse NOX4-glutathione S transferase (299–515, Prof Abboud HE, University of Texas);

2. goat polyclonal antibodies to:

- RAGE (Novus Biologicals, ab7764) ;

3. rat monoclonal antibodies to:

- mouse F4/80 (Novus Biologicals, NB 600-404);

4. mouse monoclonal antibody to:

- CML (biotinylated) (Wako, Neuss, Germany);

Secondary antibodies:

1. Biotinylated Goat Anti-Rabbit Immunoglobulins (Dako, E0432)
2. Biotinylated Rabbit polyclonal to Goat IgG H&L (Abcam, ab6740)
3. Biotinylated Goat polyclonal to Rat IgG H&L (Abcam, ab6844)
4. Biotinylated Goat polyclonal to mouse IgG H&L (Abcam, ab6788)

3.7 Quantitative real time PCR

Total RNA was extracted from mice renal cortex, human kidney specimens and mice liver with the RNAeasy mini kit (Qiagen, Milan, Italy). Then, 1μg of RNA was reverse-transcribed in a 20-μl reaction tube using High Capacity cDNA Reverse Transcription Kit (Applied Biosystems, Monza, Italy). Quantitative PCR was performed in triplicate on an ABI PRISM 7900 HT instrument (Applied Biosystems) following the standard protocol. Transcripts for fibronectin, collagen IV α1 chain, MCP-1, F4/80, collagen I, TGF- β, CXCR3, RAGE, TNF α, ACC, FAS, SREBP-1c, CPT1, LXR α, LXR β, $P2X_7R$, NLRP3, ASC, pro-caspase-1, pro-IL-1β and pro-IL-18 were quantified by TaqMan Gene Expression Assays (Applied Biosystems) using the primers reported in Table 1. Amplifications were normalized by β-actin and quantitation of gene expression was performed using the ΔΔCT calculation, where CT is the threshold cycle. The amount of the target gene, normalized to β-actin and relative to the calibrator (sample from a WT animal or a nondiabetic individual) was given as 2- ΔΔCT. A standard curve for each gene was constructed using multiple dilutions of the calibrator. Standard curves were accepted only if the slope was approximately -3, with an r value >0.98, and were used to estimate PCR efficiency. Results were analyzed using the SDS 2.1 Applied Biosystems software.

Mouse taqman assays	code
ACT β	Mm00607939_s1
COLL IV	Mm00802377_m1
CXCR3	Mm00438354_m1
F4/80	Mm00802529_m1
FN	Mm00692666_m1
MCP1 (Ccl2)	Mm00441242_m1
NLRP3	Mm00840904_m1
P2X7R	Mm00440578_m1
RAGE	Mm00545815_m1
TNFα	Mm99999058_m1
TGFβ	Mm01178820_m1
IL1β	Mm00434228_m1
IL 18	Mm00434225_m1
casp1	Mm00438023_m1
COLL I	Mm00801666_g1
ACC	Mm01304257_m1
FAS	Mm00662319_m1
SREBP 1c	Mm00550338_m1
CPT 1	Mm01231183_m1
LXR α	Mm00443451_m1
LXR β	Mm00437262_m1

Human taqman assays	code
NLRP3	Hs 00918082_m1
P2X7R	Hs00175721_m1
ACT β	Hs99999903_m1

Table 1. Mouse and human taqman assays

3.8 Statistical analysis

Results are expressed as means ± SD or median and interquartile range. Comparisons between two groups were performed using the Student's t test or the Mann-Whitney U-test for parametric and nonparametric data, respectively. One-way ANOVA was used to compare multiple groups, followed by the Student–Newman–Keuls post hoc test for multiple comparisons. A P value of <0.05 was considered statistically significant.

Results

4.1 Animal kidney studies

4.1.1 Metabolic parameters. To assess whether $P2X_7R$ ablation had any impact on the metabolic status of both NFD and HFD-fed mice, thus introducing possible confounding effects on the direct role of the $P2X_7R$ on HFD-induced renal and liver injury, we evaluated the metabolic profile of $P2X_7R^{-/-}$ and coeval C57/BL6 WT mice fed a HFD or a NFD (*Table 1*). Body weights, but not kidney weights, were significantly higher in mice on a HFD, as compared with animals fed a NFD. Likewise, blood glucose and insulin concentrations, the HOMA-IR index, and triglyceride and cholesterol levels were higher in HFD- vs. NFD-fed mice, with no difference between the two genotypes.

	WT-NFD	$P2X_7R^{-/-}$-NFD	WT-HFD	$P2X7R^{-/-}$-HFD
Body weight (g)	31.00±4.20	33.45±2.84	40.29±6.99 *	39.00±4.65 *
Glucose, mmol/l	5.05±0.78	5.19±0.55	7.41±0.90 *	7.42±0.67 *
Insulin, pmol/L	53.8±15.9	52.5±10.6	146.3±14.3 *	143.3±14.2 *
HOMA-IR	1.64±0.34	1.68±0.32	6.70±0.84 *	6.61±1.09 *
Cholesterol, mmol/l	2.45±0.16	2.49±0.33	3.88±0.31 *	3.82±0.40 *
Triglycerides, mmol/l	0.49±0.10	0.47±0.13	1.37±0.15 *	1.36±0.16 *
Kidney weight, g	0.196±0.021	0.211±0.042	0.217±0.026	0.224±0.035

Table 1. Metabolic parameters. Body and kidney weights, blood glucose, serum insulin, homeostasis model assessment - insulin resistance (HOMA-IR) index, plasma cholesterol and triglycerides in wild type (WT) and $P2X_7R$ knockout ($P2X_7R^{-/-}$) mice fed a normal-fat diet (NFD) or a high-fat diet (HFD) (mean±SD; n=7 per group). * $P<0.001$ vs. NFD-fed mice.

4.1.2 Renal function and structure. In order to evaluate the impact of $P2X_7R$ ablation on renal disease, we then assessed the functional and structural alterations induced by the HFD in the two genotypes. Serum creatinine levels did not differ among the experimental groups, whereas proteinuria and albuminuria increased significantly only in the WT animals on a HFD (*Table 2*).

	WT-NFD	$P2X_7R^{-/-}$-NFD	WT-HFD	$P2X7R^{-/-}$-HFD
Serum creatinine, µmol/l	28.95±2.43	28.51±4.04	28.58±2.20	28.73±2.75
Urinary PC, mg/g	2.11 ± 0.14	2.07 ± 0.19	3.53 ± 0.91 *	2.54 ± 0.36 †
Urinary AC, mg/g	1.19±0.16	1.21±0.10	2.27±0.41 *	1.58±0.19 ‡

Table 2. Renal function parameters. Serum creatinine and urinary protein/creatinine (PC) and albumin/creatinine (AC) ratio in wild type (WT) and $P2X_7R$ knockout ($P2X_7R^{-/-}$) mice fed a normal-fat diet (NFD) or a high-fat diet (HFD) (mean±SD; n=7 per group). * $P<0.001$ vs. NFD-fed mice; or † $P<0.001$ or ‡ $P<0.05$ vs. WT mice.

Morphometric analysis of PAS-stained kidney sections revealed that the HFD induced glomerular hypertrophy and mesangial expansion in WT mice, as indicated by the significant increase of mGA, fMA and mMA, as compared with animals fed a NFD. Conversely, $P2X_7R^{-/-}$ mice were partially protected from the injurious effects of the HFD (*Figure 1*).

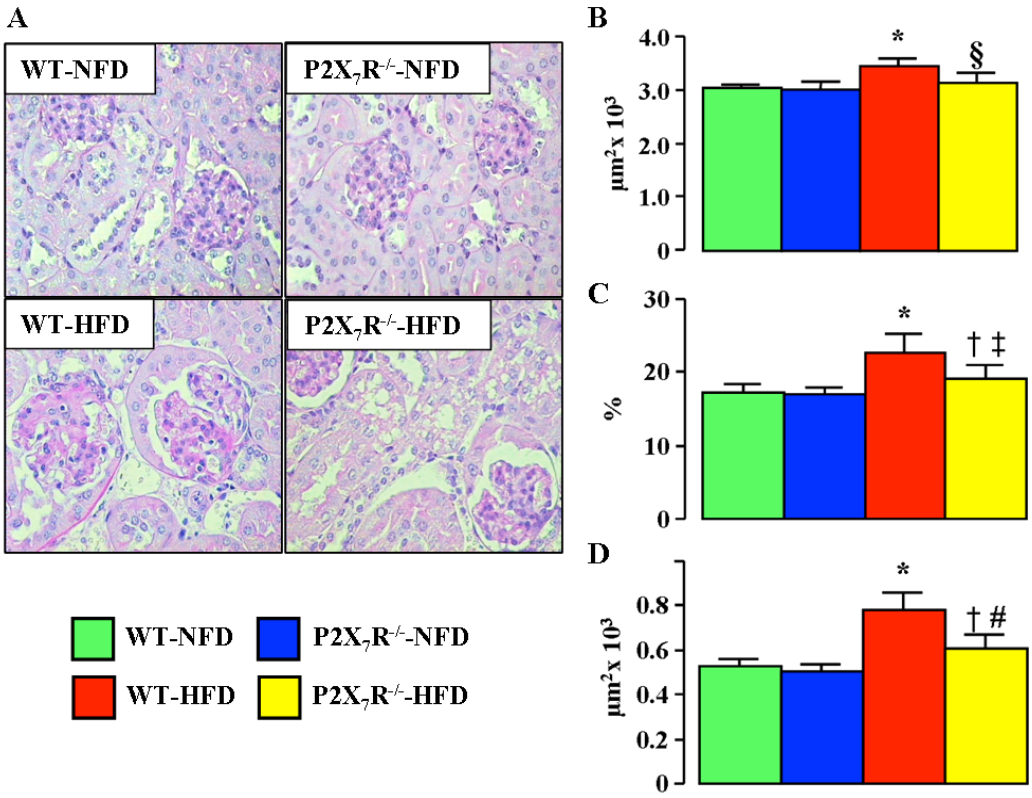

Figure 1: Glomerular morphology and morphometry. PAS staining of kidney sections from representative WT and $P2X_7R^{-/-}$ mice fed a NFD or a HFD (*Panel A*; original magnification 400x); and quantification of mGA (*Panel B*), fMA (*Panel C*), and mMA (*Panel D*) in WT and $P2X_7R^{-/-}$ mice fed a NFD or a HFD (mean±SD; n=6-7 per group). * P<0.001 or † P<0.05 vs. NFD-fed mice; ‡ P<0.001, § P<0.01 or # P<0.05 vs. WT mice. PAS = periodic acid Schiff; WT = wild type; $P2X_7R^{-/-}$ = knockout for $P2X_7$ receptor; NFD = normal fat diet; HFD = high fat diet; mGA = mean glomerular area; fMA = fractional mesangial area; mMA = mean mesangial area.

4.1.3 Renal/glomerular apoptosis, fibrosis, inflammation and lipid accumulation. We then examined the effect of $P2X_7R$ deficiency on the fundamental processes driving the development of renal disease. Glomerular cell apoptosis increased significantly (2.5-fold) only in the WT mice on a HFD (*Figure 2, panel A and B)*. Glomerular expression of fibronectin and collagen IV α1 chain were also increased in HFD-fed mice, with significantly lower values in $P2X_7R^{-/-}$ vs. WT animals (*Figure 2, panel C,D,E and G*). The pro-fibrotic effect of the HFD was blunted in $P2X_7R^{-/-}$ mice also at the transcriptional level (*Figure 2, panel F and H*).

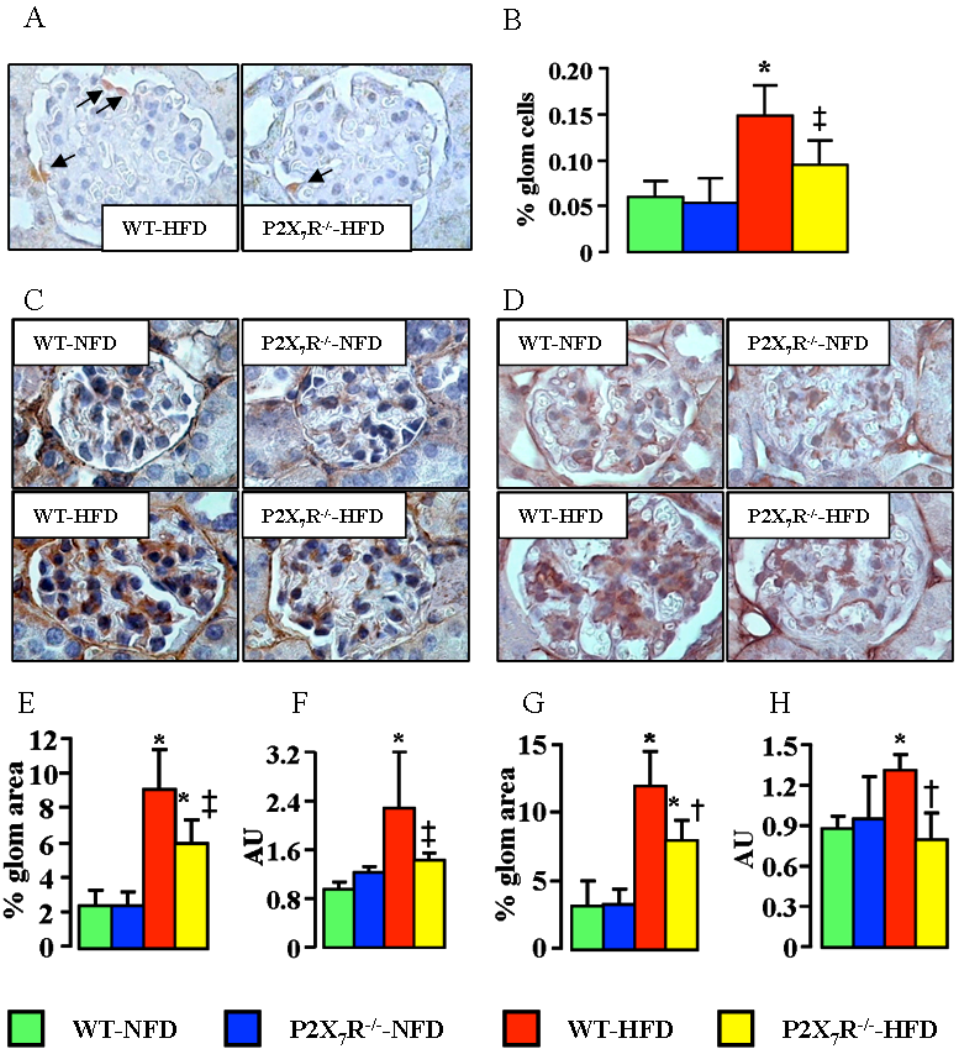

Figure 2: Glomerular cell and ECM turnover. Immunohistochemistry for active caspase-3 from representative WT and $P2X_7R^{-/-}$ mice fed a HFD (*Panel A*, arrows =positive cells; original magnification 1,000x) and quantification of glomerular cell apoptosis in WT and $P2X_7R^{-/-}$ mice fed a NFD or a HFD (*Panel B*); immunohistochemistry for fibronectin (*Panel C*) and collagen IV α1 chain (*Panel D*) from representative WT and $P2X_7R^{-/-}$ mice fed a NFD or a HFD (original magnification 1,000x), and quantification of fibronectin and collagen IV glomerular protein content (*Panels E* and *G*) and kidney cortex mRNA expression (*Panels F* and *H*) in WT and $P2X_7R^{-/-}$ mice fed a NFD or a HFD (mean±SD; n=4-6 per group). * P<0.001 vs. NFD-fed mice; † P<0.001 or ‡ P<0.01 vs. WT mice. WT = wild type; $P2X_7R^{-/-}$ = knockout for $P2X_7$ receptor; HFD = high fat diet; NFD = normal fat diet.

Furthermore, in response to the HFD, renal cortex protein and mRNA levels of the inflammatory markers F4/80 (*Figure 3, panel A, C and E*) and MCP-1 (*Figure 3, panel B, D and F*) increased markedly in the WT animals, and these changes were significantly attenuated in $P2X_7R^{-/-}$ mice.

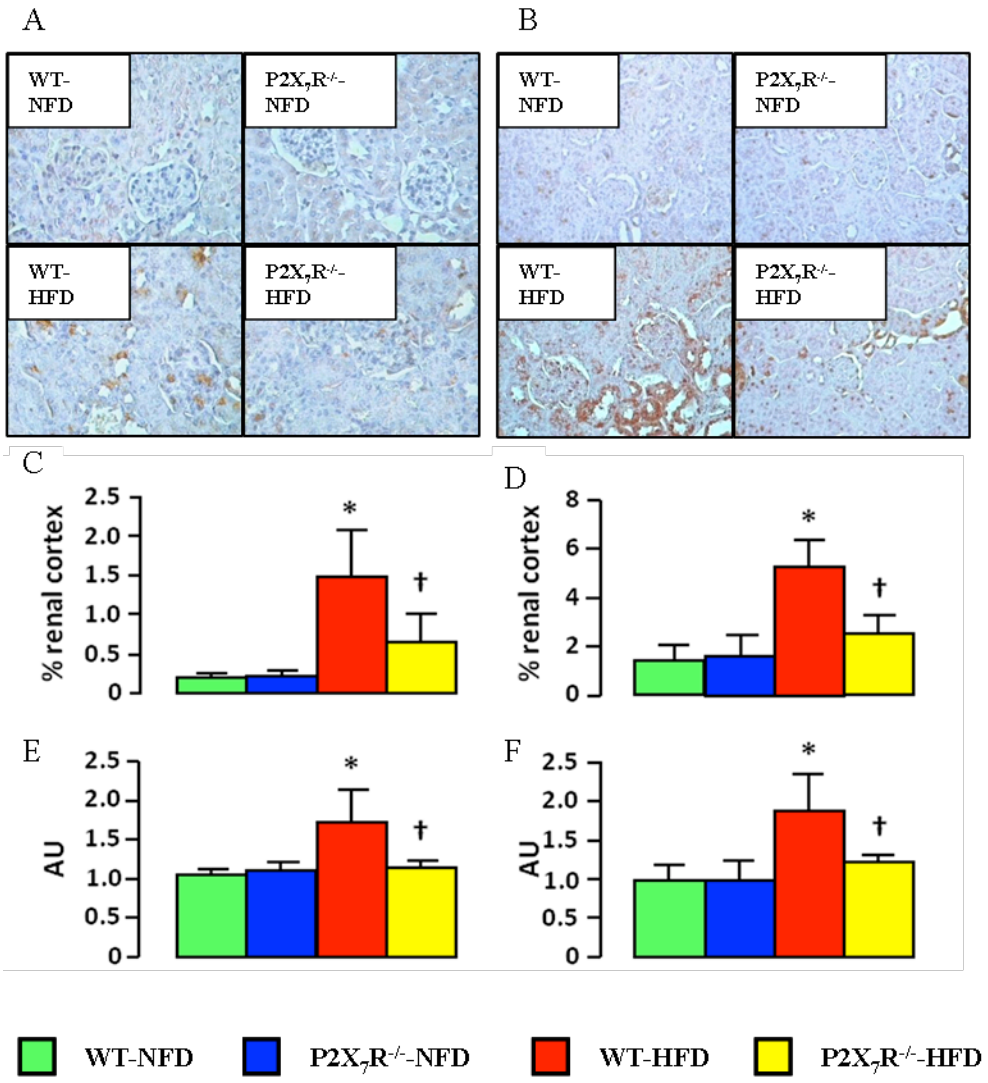

Figure 3: Renal inflammation. Immunohistochemistry for F4/80 (*Panel A*; original magnification 400x) and MCP-1 (*Panel B*; original magnification 250x) from representative WT and $P2X_7R^{-/-}$ mice fed a NFD or a HFD, and quantification of renal cortex protein content of F4/80 (*Panel C*) and MCP-1 (*Panel D*) and mRNA expression of F4/80 (*Panel E*) and MCP-1 (*Panel F*), in WT and $P2X_7R^{-/-}$ mice fed a NFD or a HFD (mean±SD; n=4-6 per group). * P<0.001 vs. NFD-fed mice; † P<0.001 vs. WT mice. MCP-1 = monocyte chemoattractant protein 1; WT = wild type; $P2X_7R^{-/-}$ = knockout for $P2X_7$ receptor; NFD = normal fat diet; HFD = high fat diet.

Finally, ORO staining revealed that the HFD induced marked neutral lipid accumulation in the tubular compartment and, to a lesser extent, in the glomeruli, with no difference between the two genotypes (*figure 4*).

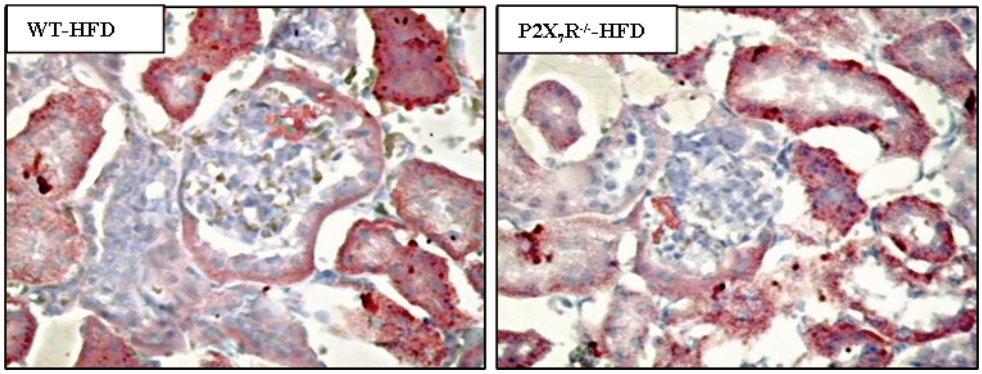

Figure 4: Renal lipid accumulation. ORO staining (original magnification 400x) from representative WT and $P2X_7R^{-/-}$ mice fed a HFD. WT = wild type; $P2X_7R^{-/-}$ = knockout for $P2X_7$ receptor; HFD = high fat diet.

4.1.4 Renal oxidative and carbonyl stress. In view of the recent finding that $P2X_7R$ is a primary mediator of oxidative stress-induced exacerbation of inflammatory tissue injury via NADPH oxidase-dependent mechanisms, as well as of the role of ROS as activators of the NLRP3 inflammasome, we also evaluated the protein expression level of Nox4, the major NADPHox isoform of the kidney, and several markers of tissue oxidative and carbonyl stress. On a HFD, Nox4 was markedly up-regulated in WT and to a significantly lower extent in $P2X_7R^{-/-}$ mice (*Figure 5, panel A and B*). Similar results were obtained for the activation of NF-kB/p65 (*Figure 5, panel C*). Consistently, the glomerular content of CML (*Figure 5, panel D and E*) and HNE adducts (*Figure 5, panel F and G*) as well as the protein expression of RAGE (*Figure 5, panel H and I*) were higher in mice fed a HFD as compared with those on a NFD, again to a significantly lower extent in $P2X_7R^{-/-}$ vs. WT mice.

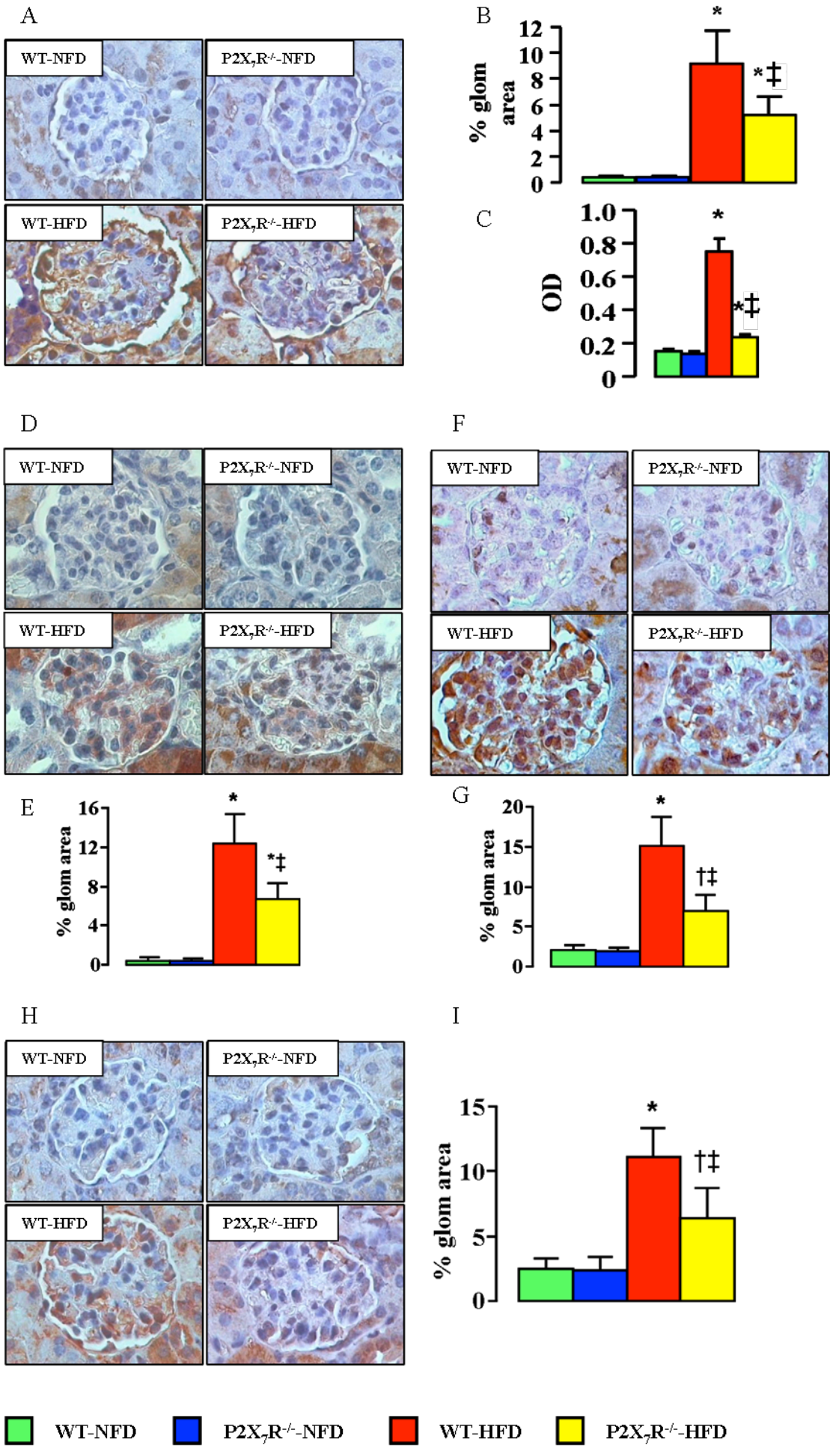
A
WT-NFD
P2X7R-/--NFD
WT-HFD
P2X7R-/--HFD
B
% glom area
0
2
4
6
8
10
12
*
*‡
C
OD
0
0.2
0.4
0.6
0.8
1.0
*
*‡
D
WT-NFD
P2X7R-/--NFD
WT-HFD
P2X7R-/--HFD
F
WT-NFD
P2X7R-/--NFD
WT-HFD
P2X7R-/--HFD
E
% glom area
0
4
8
12
16
*
*‡
G
% glom area
0
5
10
15
20
*
††
H
WT-NFD
P2X7R-/--NFD
WT-HFD
P2X7R-/--HFD
I
% glom area
0
5
10
15
*
††
WT-NFD
P2X7R-/--NFD
WT-HFD
P2X7R-/--HFD

Figure 5: Renal oxidative and carbonyl stress and NF-kB activation. Immunohistochemistry for Nox4 (*Panel A*), CML (*Panel D*), HNE adducts (*Panel F*) and RAGE (*Panel H*) from representative WT and $P2X_7R^{-/-}$ mice fed a NFD or a HFD (original magnification 1,000x), and quantification of renal cortex protein content of Nox4 (*Panel B*), CML (*Panel E*), HNE adducts (*Panel G*) and RAGE (*Panel I*); activation of NF-κB (*Panel C*) in WT and $P2X_7R^{-/-}$ mice fed a NFD or a HFD (mean±SD; n=4-6 per group). * P<0.001 vs. NFD-fed mice; † P<0.01 vs. NFD-fed mice; ‡ P<0.001 vs. WT mice. Nox4 = renal isoform 4 of NAD(P)H oxidase; WT = wild type; $P2X_7R^{-/-}$ = knockout for $P2X_7$ receptor; NFD = normal fat diet; HFD = high fat diet; NFκB = nuclear factor κB; CML = Nε-(carboxymethyl)lysine; HNE = 4-hydroxynonenal; RAGE = receptor for AGEs.

4.1.5 Renal expression and activation of the $P2X_7R$/NLRP3 axis. Finally, we assessed whether the $P2X_7R$/NLRP3 axis was activated in response to the HFD and whether the expression/activation of the NLRP3 inflammasome was affected by deletion of the $P2X_7R$ gene. $P2X_7R$ and NLRP3 expression data are presented in *Figure 6*, whereas the renal expression of NLRP3-associated molecules and activation of the NLRP3 inflammasome are shown in *Figure 7*. Only a very low positivity for $P2X_7R$ was detected at the tubular level in WT mice fed a NFD. $P2X_7R$ staining increased in mice on a HFD, both at the tubular level, where the distal tubules and macula densa showed the most intense positivity, and at the glomerular level, where a positive staining was observed in mesangial cells and especially podocytes. (*Figure 6, panel A, B and C*). Likewise, renal cortex mRNA expression of $P2X_7R$ were significantly higher in HFD- vs. NFD-fed WT animals, as assessed by RT-PCR (*Figure 6, panel D*).

Immunohistochemistry revealed mild tubular staining of NLRP3 in both WT and $P2X_7R^{-/-}$ mice on a NFD. NLRP3 positivity increased significantly in HFD-fed animals, showing also glomerular staining, though it was significantly lower in $P2X_7R^{-/-}$ vs. WT mice (*Figure 6, panel E, F and G*). Moreover, NLRP3 mRNA levels were significantly increased in the renal cortex of WT, but not of $P2X_7R^{-/-}$ mice fed a HFD (*Figure 6, panel H*).

Likewise, the gene expression level of the inflammasome components and substrates ASC, pro-caspase-1, pro-IL-1β and pro-IL-18 increased significantly only in HFD-fed WT mice (*Figure 7, panel A, B, C and D*). Western blot analysis of caspase-1 in renal cortex extracts showed that the 45 kD subunit (pro-caspase-1) increased significantly in response to the HFD in WT, but not in $P2X_7R^{-/-}$ mice, whereas the 20 kD subunit (active caspase-1) was detectable only in HFD-fed mice and was significantly lower in $P2X_7R^{-/-}$ vs. WT animals, as the caspase-1:pro-caspase-1 ratio (*Figure 7, panel E and F*). Also renal cortex IL-1β and IL-18 protein

levels, as assessed by ELISA, increased significantly in HFD-fed mice and increments were significantly lower in $P2X_7R^{-/-}$ vs. WT animals (*Figure 7, panel G and H*).

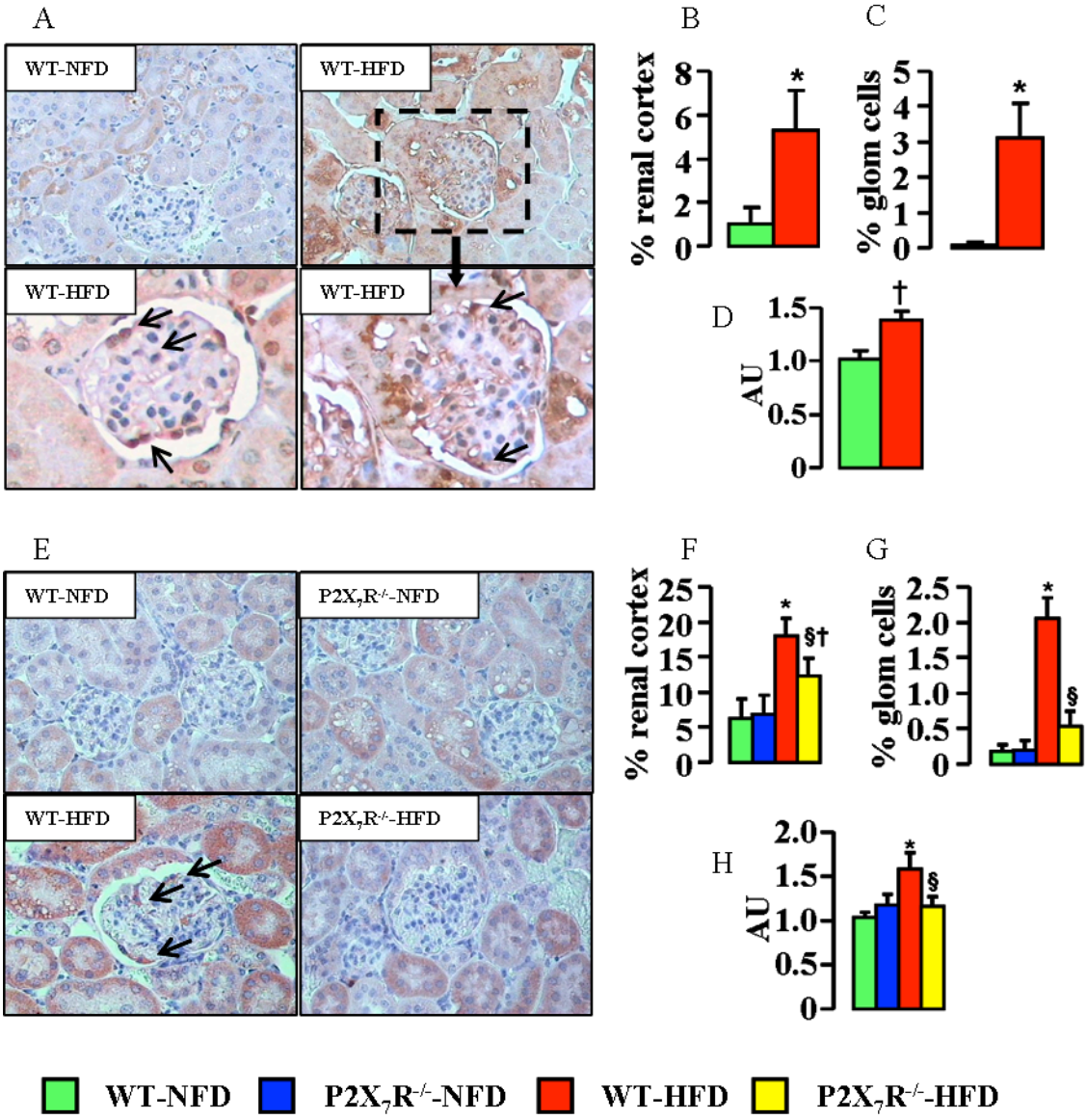

Figure 6: Renal/glomerular expression of $P2X_7R$ and NLRP3. Immunohistochemistry for $P2X_7R$ (*Panel A*; original magnification 400x top, 1,000x bottom) from representative WT mice fed a NFD or a HFD and for NLRP3 (*Panel E*; original magnification 400x) from representative WT and $P2X_7R^{-/-}$ mice fed a NFD or a HFD (arrows =positive cells) and quantification of renal cortex protein content and glomerular cell of $P2X_7R$ (*Panels B-C*) and NLRP3 (*Panels F-G*) positivity; renal cortex mRNA expression of $P2X_7R$ (*Panel D*) and NLRP3 (*Panel H*) in WT and $P2X_7R^{-/-}$ mice fed a NFD or a HFD (mean±SD; n=4 per group) * P<0.001, † P<0.01 vs. NFD-fed mice; § P<0.001 vs. WT mice. NLRP3 = nucleotide-binding oligomerization domain, leucine-rich repeat and pyrin domain containing 3; WT = wild type; $P2X_7R^{-/-}$ = knockout for $P2X_7$ receptor; NFD = normal fat diet; HFD = high fat diet.

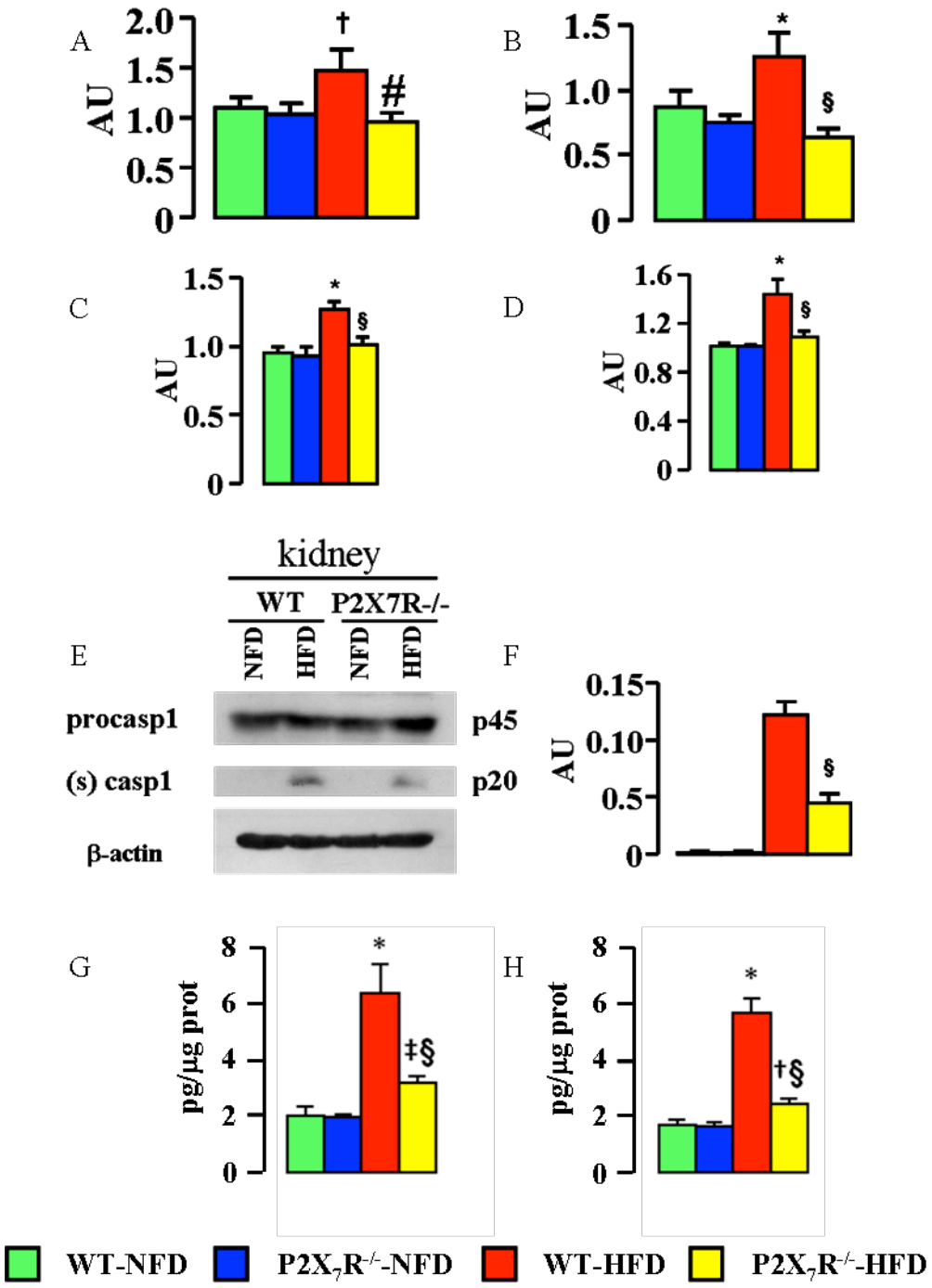

Figure 7: Renal expression of NLRP3-associated molecules and activation of the NLRP3 inflammasome. Renal cortex mRNA expression of ASC (*Panel A*), caspase-1 (*Panel B*), pro-IL-1β (*Panel C*) and pro-IL-18 (*Panel D*); representative Western blot for pro-caspase-1, caspase-1 and β-actin renal cortex protein expression (*Panel E*), and quantification of caspase-1/pro-caspase-1 ratio (*Panel F*); and renal cortex levels of IL-1β (*Panel G*) and IL-18 (*Panel H*) in WT and $P2X_7R^{-/-}$ mice fed a NFD or a HFD (mean±SD; n=4 per group). * P<0.001, † P<0.01 or ‡ P<0.05 vs. NFD; § P<0.001 or # P<0.01 vs. WT. NLRP3 = nucleotide-binding oligomerization domain, leucine-rich repeat and pyrin domain containing 3; ASC = apoptosis-associated speck-like protein containing a caspase recruitment domain; IL = interleukin; WT = wild type; $P2X_7R^{-/-}$ = knockout for $P2X_7$ receptor; NFD = normal fat diet; HFD = high fat diet.

4.2 Human kidney studies

We finally investigated whether the $P2X_7R$-NLRP3 axis was indeed activated also in kidneys from 6 type 2 diabetic subjects, as compared with 3 non-diabetic individuals (*Figure 8*). All diabetic subjects except one showed histological features consistent with stage 2 or 3 diabetic nephropathy, i.e. glomerular hypertrophy and mild to severe mesangial expansion in more than 25% of total mesangium observed throughout the sample. Conversely, only one control subject, who had a history of hypertension, showed renal lesions (arteriosclerosis) at histological examination (*Figure 8, panel A*).

Immunohistochemistry revealed an increased positivity for $P2X_7R$ (*Figure 8, panel A, B and C*) and NLRP3 (*Figure 8, panel A, D and E*) in kidneys from diabetic vs. non-diabetic subjects, with a staining pattern resembling that observed in mice. The mRNA levels of $P2X_7R$, NLRP3 and ASC were also significantly higher in patients with type 2 diabetes (*Figure 8, panel F, G and H*). Interestingly, the non-diabetic subject with renal lesions had protein and mRNA expression values similar to those of diabetic individuals, whereas the diabetic patient with no lesions showed values within the range of controls, consistent with the histological features.

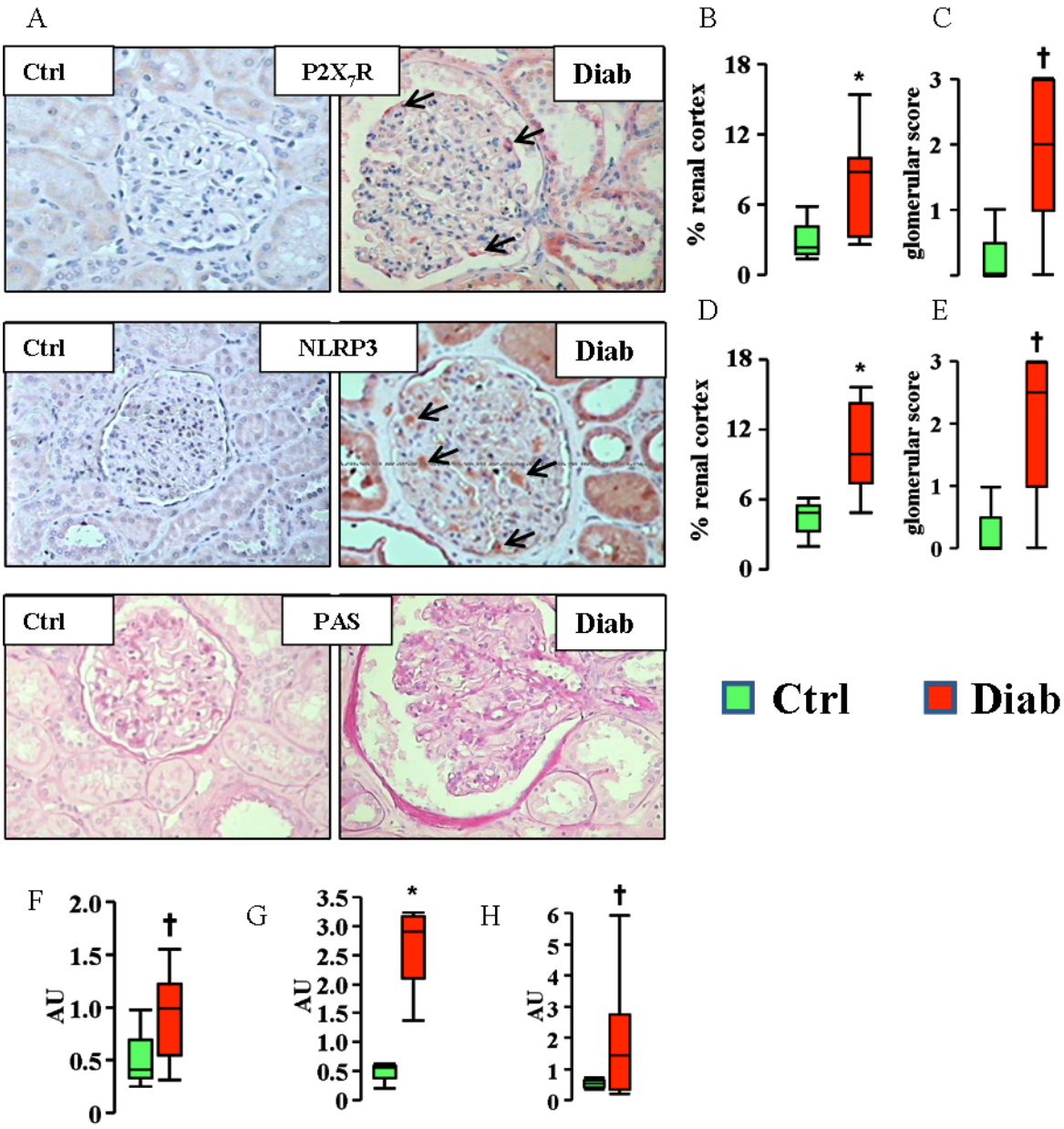

Figure 8: Human renal tissue P2X$_7$R/NLRP3 inflammasome system. Immunohistochemistry for P2X$_7$R and NLRP3 and PAS staining of representative kidney sections from non-diabetic control (Ctrl) and diabetic (Diab) subjects (*Panel A*, arrows =positive cells; original magnification 250x), and quantification of renal cortex and glomerular protein content of P2X$_7$R (*Panels B-C*) and NLRP3 (*Panels D-E*), and renal mRNA expression of P2X$_7$R (*Panel F*), NLRP3 (*Panel G*) and ASC (*Panel H*) in non-diabetic control (n=3) and diabetic (n=6) subjects (median and interquartile range). * P<0.01 or † P<0.05 vs. Ctrl. P2X$_7$R = P2X$_7$ receptor; NLRP3 = nucleotide-binding oligomerization domain, leucine-rich repeat and pyrin domain containing 3; ASC = apoptosis-associated speck-like protein containing a caspase recruitment domain.

4.3 Animal liver studies

4.3.1 Liver function. In order to evaluate the impact of $P2X_7R$ ablation on HFD-induced liver disease, we first assessed the functional alterations induced by the HFD in the two genotypes. The cytolytic markers aspartate transaminase (AST) and alanine transaminase (ALT) increased in the animals mice fed the HFD of both genotypes, although the $P2X_7R^{-/-}$ mice showed significantly lower values as compared with WT, indicating reduced liver damage (*Table 3*).

	WT-NFD	$P2X_7R^{-/-}$-NFD	WT-HFD	P2X7R$^{-/-}$-HFD
AST (IU/L)	32.62±4.05	31.54±4.22	82.16±12.04 *	54.12±8.87 * †
ALT (IU/L)	18.05 ± 5.01	17.58 ± 3.48	104.54 ± 15.25 *	49.21± 7.77 * †

Table 3. AST and ALT parameters. AST and ALT in NFD- and HFD-fed WT and $P2X_7R^{-/-}$-mice (mean ± SD; n = 7 per group). *P<0.001 vs. NFD; †P<0.001 vs. WT.

4.3.2 Steatosis grading. By the examination of hematoxylin and eosin-stained sections, steatosis was detected only in HFD-fed mice, but it was of higher grade in WT than in $P2x_7R^{-/-}$ mice. In detail, WT HFD mice were ranked in all three grades showing predominant grade 3 steatosis. Conversely, $P2X_7R^{-/-}$ HFD mice were partially protected from the accumulation of lipids, with 4 on 7 mice showing grade 1 steatosis (*Figure 9, panel A and C*).

4.3.3 NAFLD classification $P2x_7R^{-/-}$ mice were protected from NAFLD. In fact, while 4 on 7 (57%) WT-HFD mice showed stage 3 (mixed steatosis with lobular inflammation and ballooning degeneration) and 4 NAFLD (mixed steatosis with lobular inflammation and ballooning degeneration and macrovesicular steatosis, associated with portal and lobular inflammation, Councilman's bodies, ballooning degeneration, Mallory's hyaline, and fibrosis), only 1 on 7 (14%) $P2x_7R^{-/-}$ animal fell into stage 3. The remaining 6 $P2X_7R^{-/-}$ mice did not fulfill NASH criteria, with 1 animal showing stage 2 (predominantly microvesicular steatosis with mild lobular inflammation) and 5 animals showing stage 1 (simple steatosis) NAFLD (*Figure 9, panel A, B and D*).

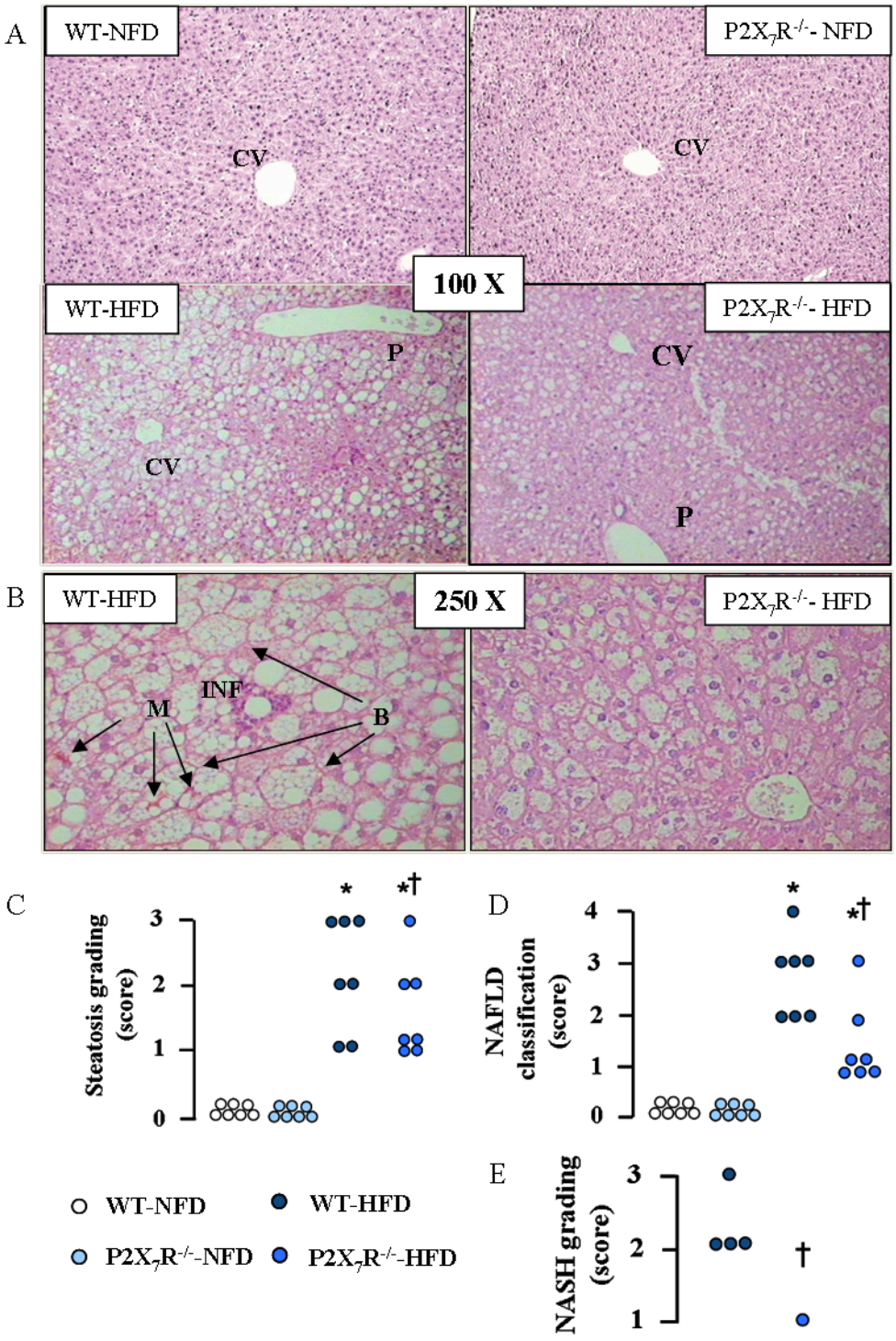

Figure 9. Steatosis grading, NAFLD classification and NASH grading. Liver sections from representative HFD-fed WT and $P2X_7R^{-/-}$ mice stained with hematoxylin and eosin (*Panel A*; original magnification 100x, *Panel B,* 250x) and steatosis grading (*Panel C*), NAFLD classification (*Panel D*) and NASH grading (*Panel E*) in NFD- and HFD-fed WT and $P2X_7R^{-/-}$ mice (mean ± SD; n = 7 per group except E, HFD-fed WT- n=4 and $P2X_7R^{-/-}$ n=1 mice fulfilling NASH criteria). p = portal area; CV = centrolobular vein; B = ballooning degeneration; M = Mallory's body; INF = inflammation. * p <0.001 vs. NFD-fed mice; † p <0.05 vs. WT mice. WT = wild type; $P2X_7R^{-/-}$ = knockout for P2X7 receptor; NFD = normal fat diet; HFD = high fat diet.

4.3.4 NASH grading and staging Of the 4 WT-HFD animals classified as having NASH, 3 showed grade 2 (moderate) and 1 grade 3 (severe or florid) NASH, whereas 1 exhibited stage 2 (zone 3 portal/periportal, perivenular/centrolobular, perisinusoidal/pericellular fibrosis; focal or extensive) and 3 stage 1 (i.e. as stage 2, except portal fibrosis) fibrosis, as assessed by the analysis of Masson's trichrome stained sections. The sole $P2X_7R^{-/-}$ mice fulfilling NASH criteria was graded 1 (mild) for NASH and staged 1 for fibrosis. (*Figure 9, panel E; Figure 10, panel A and B*)

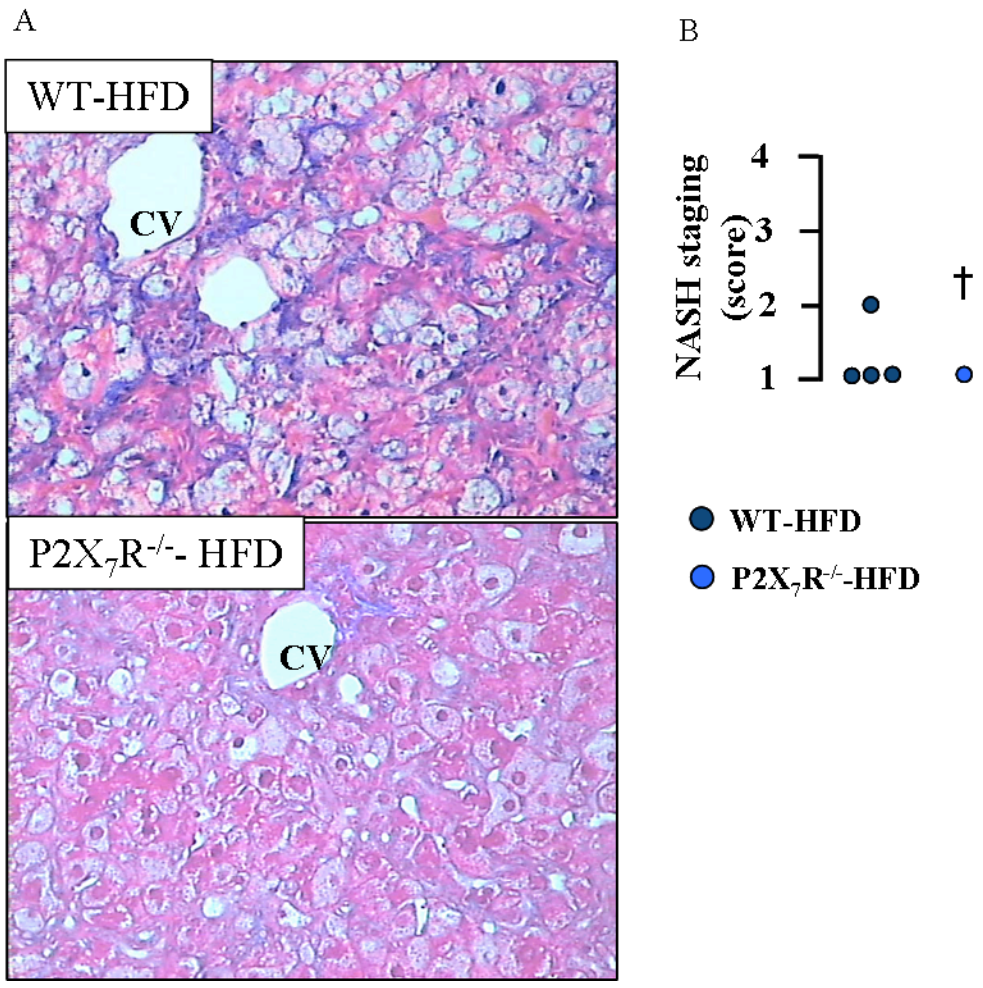

Figure 10. NASH staging. Liver sections from representative HFD-fed WT and $P2X_7R^{-/-}$ mice stained with Masson's trichrome (*Panel A*; original magnification 250x) and NASH staging (*Panel B*) in HFD-fed WT (n= 4) and $P2X_7R^{-/-}$ (n= 1) mice fulfilling NASH criteria. The blue color represents collagen. WT-HFD mice show perisinusoidal/pericellular and perivenular/centrolobular fibrosis. In contrast, $P2X_7R^{-/-}$ -HFD mice show no, or very mild, blue staining, indicating a preserved stromal architecture of the liver. mean ± SD. CV = centrolobular vein. † $p < 0.05$ vs. WT mice. WT = wild type; $P2X_7R^{-/-}$ = knockout for P2X7 receptor; HFD = high fat diet.

4.3.5 Liver inflammation, fibrosis and lipid metabolism. We then examined the effect of $P2X_7R$ deficiency on the fundamental processes driving the development of liver disease, such as inflammation, fibrosis and lipid metabolism. Transcriptional expression of liver inflammatory markers MCP-1, TNF-α and CXCR3 were increased in HFD-fed mice, with significantly lower values in $P2X_7R^{-/-}$ vs. WT animals (*Table 4, A*). Furthermore, in response to the HFD, mRNA levels of the collagen I, fibronectin and TGF-β increased markedly in the WT animals, and these changes were significantly attenuated in $P2X_7R^{-/-}$ mice (*Table 4, B*). Finally, transcriptional levels of genes implicated in the lipid metabolism of the liver, particularly in the lipogenesis, were assessed. Transcriptional expression of liver fatty acid synthase (FAS) and liver x receptor (LXR)-α, a transcription factor involved in the regulation of cholesterol and fatty acid homeostasis, resulted significantly increased only in WT HFD mice; while mRNA levels of Sterol Regulatory Element-Binding Proteins (SREBP-1c) and Carnitine palmitoyltransferase I (CPT-1) were increased in both genotype fed the HFD, resulting however significantly lower in $P2X_7R^{-/-}$ mice. Conversely, Acetyl-CoA carboxylase (ACC) and LXR-β were not increased by the HFD (*Table 4, C*).

		WT-NFD	WT-HFD	$P2X_7R^{-/-}$-NFD	$P2X7R^{-/-}$-HFD
A	MCP-1	1.00±0.4	3.47±0.4*	0.79±0.04	1.30±0.26*†
	TNF-α	1.00±0.22	2±0.16 *	0.62±0.24	0.94±0.07 †
	CXCR3	1.00±0.16	3.56±0.64*	1.11±0.36	1.97±0.30 *†
B	Coll I	1.00±0.21	2.25±0.18*	0.87±0.07	1.44±0.23 *†
	FN	1.00±0.04	1.79±0.23*	0.82±0.06	1.10±0.01 †
	TGF-β	1.00±0.18	1.45±0.07*	0.97±0. 06	1.13±0.02 †
C	FAS	1.00±0.02	1.34±0.03*	0.96±0.05	1.14±0.06 †
	LXR-α	1.00±0.01	1.50±0.02*	0.87±0.13	1.23±0.05 †
	SREBP-1c	1.00±0.03	7.89±1.71*	1.41±0.04	4.09±0.71 *†
	CPT-1	1.00±0.06	3.76±0.01 *	1.47±0.17	2.84±0.32 *†
	ACC	1.00±0.01	0.93±0.06	1.00±0.04	0.95±0.11
	LXR-β	1.00±0.01	1.12±0.16	1.05±0.32	1.13±0.03

Table 4. Liver inflammation, fibrosis and lipid metabolism. Liver gene expression of inflammatory markers (panel A), fibrosis markers (panel B) and lipid metabolism genes (panel C) in NFD- and HFD-fed WT and $P2X_7R^{-/-}$ mice (mean ± SD; n =7 per group). *P<0.01 vs. NFD; †P<0.05 vs. WT

4.3.6 Liver expression of the P2X$_7$R/NLRP3 axis. Finally, we assessed whether the mRNA and protein levels of P2X$_7$R and NLRP3 were modulated in response to the HFD and whether P2X$_7$R gene ablation was able to influence the NLRP3 response to the HFD. When fed the HFD, WT mice showed increased P2X$_7$R IHC staining both at the hepatocyte and sinusoidal level (*Figure 11, panel A and B*). Likewise, liver mRNA expression of P2X$_7$R was significantly higher in HFD- vs. NFD-fed WT animals, as assessed by RT-PCR (*Figure 11, panel C*).

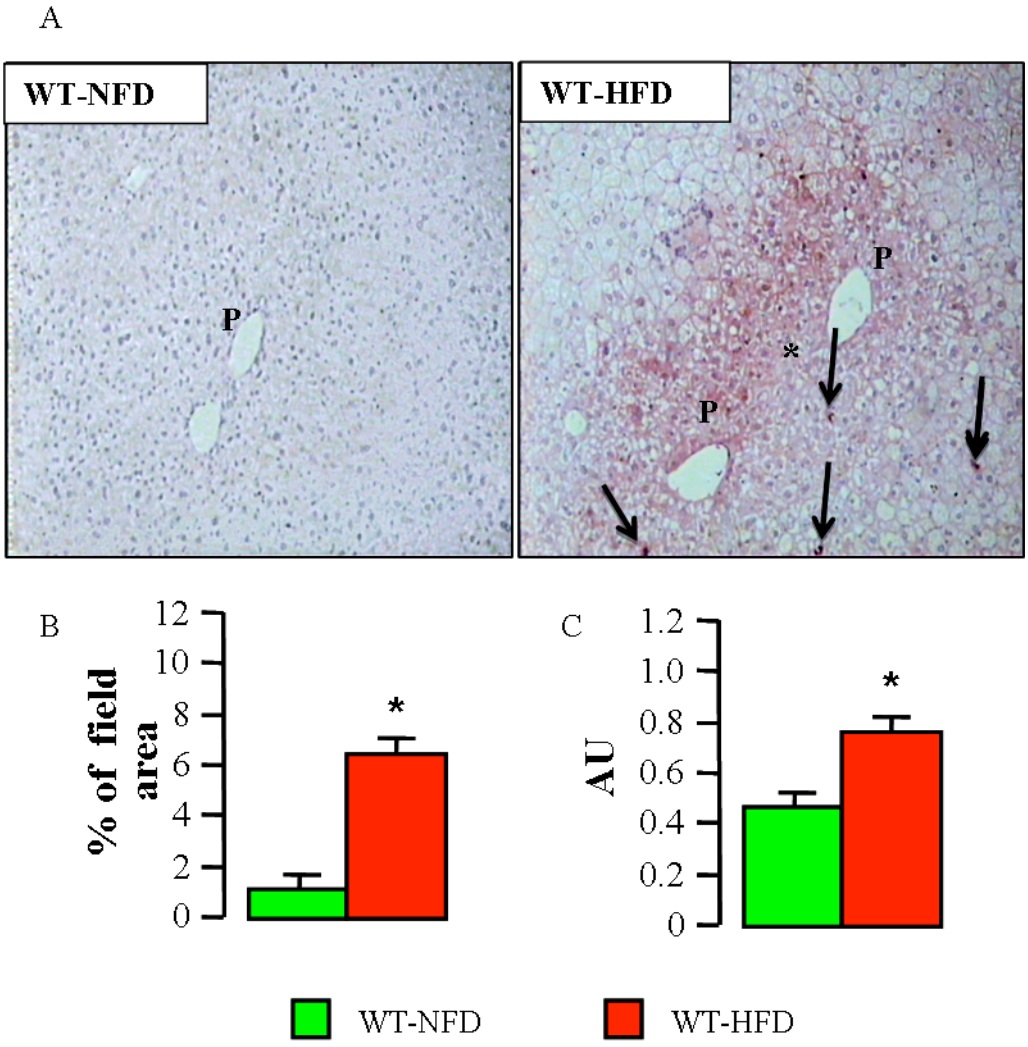

Figure 11. Liver expression of P2X7 receptor . Representative immunohistochemistry of liver P2X$_7$R (*Panel A*; original magnification 100x) in NFD-fed and HFD-fed WT mice, relative quantification (*Panel B)* by image analysis and renal cortex mRNA expression of P2X$_7$R (*Panel C*) in WT mice fed a NFD or a HFD (mean±SD; n=4 per group). Only WT-HFD mice show intense P2X$_7$R positivity (brown staining) of liver parenchymal (hepatocytes , astrisk) and non-parenchymal cells (sinusoidal lining cells, arrows), mainly around the portal tracts (P). WT = wild type; NFD = normal fat diet; HFD = high fat diet. *P<0.001 vs. NFD

Also NLRP3 protein level was increased in the liver of WT mice fed the HFD, as demonstrated by the *de novo* appearance of a strong positive staining for NLRP3 in cells lining the hepatic sinusoids, bile duct epithelial cells and infiltrating inflammatory cells. Interestingly, the NLRP3 staining of these tissue structures was virtually absent in P2X7R$^{-/-}$ HFD animals (*Figure 12, panel A*). Consistently, NLRP3 mRNA levels were significantly increased in liver of WT, but not of P2X$_7$R$^{-/-}$ mice fed a HFD (*Figure 12, panel B*)

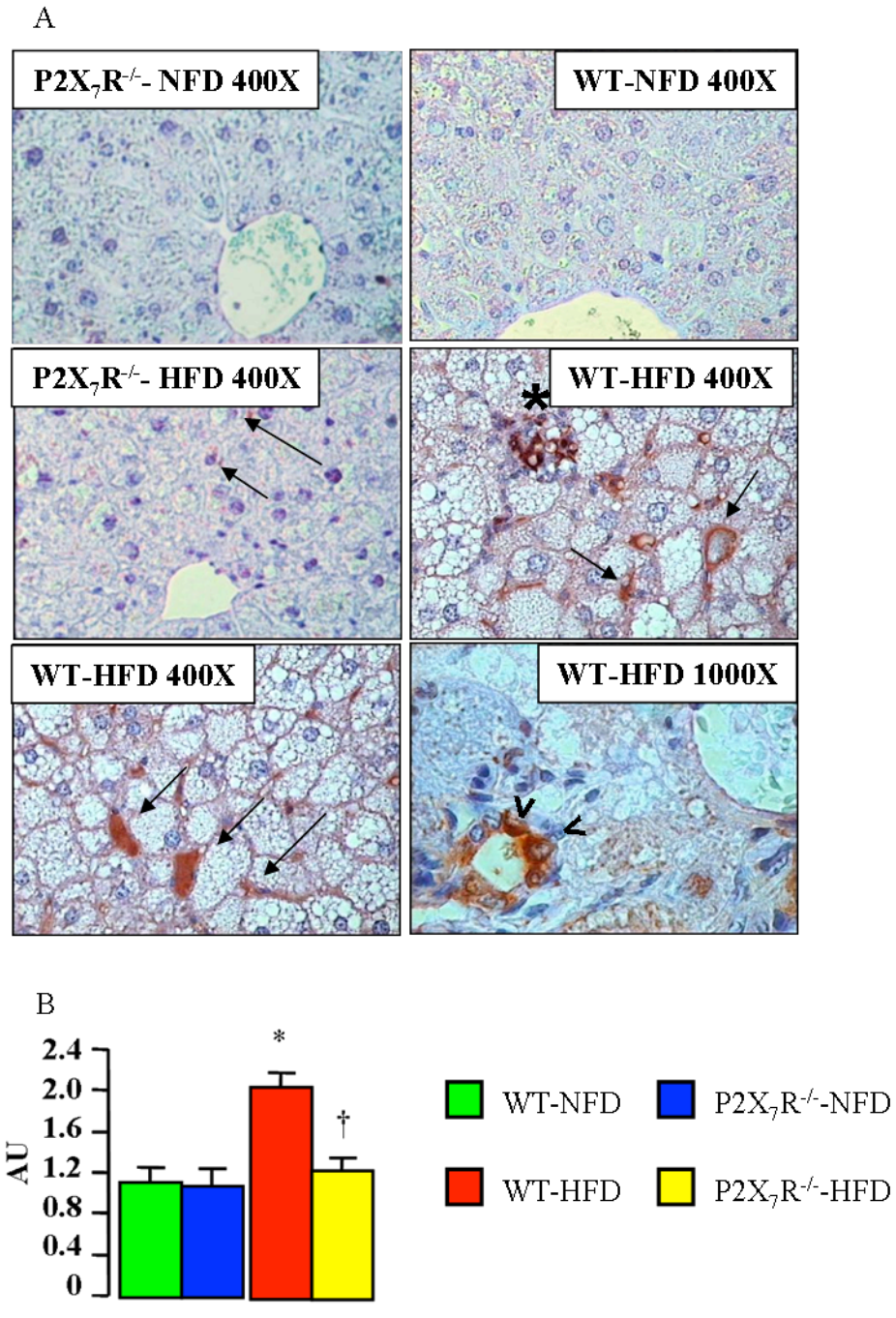

Figure 12. Liver expression of NLRP3 Representative immunohistochemistry of liver NLRP3 (*Panel A*; original magnification 400x top, 1,000x bottom) and renal cortex mRNA expression of NLRP3 (*Panel B*) in WT and $P2X_7R^{-/-}$ mice fed a NFD or a HFD (mean±SD; n=4 per group). While both WT and $P2X_7R^{-/-}$ mice on NFD show no staining for NLRP3, WT-HFD mice display intense NLRP3 inflammasome positivity (brown staining) of both resident and non-resident cells. In particular, inflammatory cells around degenerating hepatocytes (asterisk), sinusoidal (arrows) and bile duct epithelial cells (arrowheads) appear to highly express NLRP3. In contrast, only some isolated cells show faint staining for NLRP3 in $P2X_7R^{-/-}$-HFD mice. **P*<0.001 vs. NFD; †*P*<0.001 vs. WT. NLRP3 = nucleotide-binding oligomerization domain, leucine-rich repeat and pyrin domain containing 3; WT = wild type; $P2X_7R^{-/-}$ = knockout for $P2X_7$ receptor; NFD = normal fat diet; HFD = high fat diet.

Discussion

The $P2X_7$ receptor is a purinergic receptor whose pro-inflammatory role is well established. Upon activation by its ligand ATP, several downstream events follow, including secretion of pro-inflammatory interleukins and apoptosis of the cell (Wiley et al. 2011). To date, all the studies conducted on $P2X_7R^{-/-}$ mice have associated $P2X_7R$ to tissue damage induced by immune-mediated diseases, both infectious and autoimmune diseases, such as antibody-mediated glomerulonephritis (GN) (Taylor et al. 2009), and auto-immune hepatitis (Kawamura et al. 2006), or models of acute injury such as the unilateral ureteral obstruction mice model (UUO) (Gonçalves et al. 2006). To our knowledge, this study provides the first evidence that $P2X_7R$ plays a major pathogenetic role in the onset and progression of renal and liver disease induced by HFD, a mouse model of metabolic disorders characterized by a low-grade chronic inflammation.

Both WT and $P2X_7R^{-/-}$ mice fed HFD developed features characteristic of the MS, including dyslipidemia, hyperglycemia and insulin resistance. Importantly, these metabolic parameters were modified to a similar extent in WT and $P2X7R^{-/-}$ mice on a HFD, thus ruling out the possibility that protection from renal and liver injury in $P2X_7R$-deficient animals was due to a better metabolic profile.

5.1 Kidney disease. As shown by previous studies conducted on experimental animal models, a high saturated fat and/or cholesterol intake induces glomerulosclerosis and tubulo-interstitial damage (Deji et al. 2009, Iacobini et al. 2009, Kume et al. 2007, Jiang et al. 2005). Furthermore, low-grade chronic inflammation is known to play a pivotal role in central obesity and the MS (Hotamisligil 2006) as well as in the complications of these disorders, including renal disease (Krane and Wanner 2011). However, to date, the molecular basis of activation of renal pro-inflammatory and fibrogenic signaling pathways by an obesogenic high-fat diet is still poorly defined. In this work, we provide evidence that $P2X_7R$ plays a key role in the pro-inflammatory response, and consequent kidney injury, to an high fat intake. In fact, $P2X_7R^{-/-}$ mice fed HFD were partially protected by both functional and structural renal alterations, showing reduced proteinuria and albuminuria, glomerular hypertrophy and mesangial expansion and decreased glomerular apoptosis and ECM deposition. This improvement in renal structural and functional parameters was associated with reduced renal tissue

inflammation, as shown by lower renal cortex levels of the macrophage marker F4/80 and the chemokine MCP-1. Interestingly, $P2X_7R$ deletion also resulted in a blunted up-regulation of the renal NOX4 by the HFD, which is consistent with the reduced oxidative and carbonyl stress and decreased NF-*k*B activation observed in $P2X_7R^{-/-}$ mice.

In the normal kidney, $P2X_7R$ is expressed at very low levels by both glomerular and tubular cells (Gonçalves et al. 2006, Solini et al. 2005, Vonend et al. 2004). However, our data clearly show that the HFD induce an up-regulation of this purinoreceptor in the renal cortex, glomerulus included, that was associated to signs of glomerular injury, such as glomerular hypertrophy, mesangial expansion and increased apoptosis. This finding is in keeping with the observation that streptozotocin-induced diabetic rats and mice of the Ren-2 renin hypertensive strain displayed increased glomerular immunoreactivity for $P2X_7R$ (Vonend et al. 2004) and that both glucose and free fatty acids (FFAs) rapidly up-regulate $P2X_7R$ in human islets (Glass et al. 2009). However, a role for $P2X_7R$ in chronic kidney disease (CKD) was demonstrated only in the UUO model of renal injury by Goncalves et al. (2006) that, at variance with our model, is characterized by tubulo-interstitial damage of mechanical nature. In fact, they showed that $P2X_7R$ is implicated in macrophage infiltration, collagen deposition and apoptotis in response to ureteral obstruction, and that its ablation protect mice from UUO-induced renal injury. Finally, our data are in keeping with previous findings showing that $P2X_7R$ promotes mesangial cell apoptosis (Harada et al. 2000) and favors glucose-induced ECM synthesis (Solini et al. 2005).

Therefore, taken together, our data provide for the first time *in vivo* evidence for the involvement of the $P2X_7R$ in the onset and progression of CKD associated to metabolic disorders and support a role for dyslipidemia in $P2X_7R$ modulation.

5.1.1 $P2X_7R$ and NLRP3 inflammasome. Recent evidence suggests that the inflammasomes, particularly the NLRP3 inflammasome, are implicated in chronic low-grade sterile inflammation characterizing disorders like the MS (Strowig et al. 2012, Wen et al. 2012). In dietary and genetic animal models of obesity and the MS, activation of the NLRP3 inflammasome has been shown to participate in the

induction of obesity by impairing adipocyte differentiation and increasing adipocyte size (Stienstra et al. 2011, Stienstra et al. 2010) as well as in the instigation of inflammation in adipose tissue and liver (Vandanmagsar et al. 2011), thus favoring insulin resistance. However, it is still unknown which mechanisms are involved in NLRP3 activation. Our results show that NLRP3 and the inflammasome components ASC and caspase-1 were up-regulated in the kidney of WT mice fed with the HFD and that $P2X_7R$ ablation totally prevented this effect. Moreover, they provide the first evidence that $P2X_7R$ acts as an NLRP3 inflammasome activator in HFD-induced renal inflammation and injury, as evidenced by a significantly lower level of the mature forms of both caspase-1 and IL1β and 18 in $P2X_7R^{-/-}$ mice vs. WT. This is consistent with separate observations showing that ablation of either $P2X_7R$ (Gonçalves et al. 2006) or NLRP3 (Vilaysane et al. 2010) attenuate macrophage infiltration, collagen deposition and apoptosis in UUO.

The relationship between NLRP3 activation and $P2X_7R$ signaling points to a major role of the purinergic system in regulating the activity of the NLRP3 inflammasome in the kidney in response to a HFD, at variance with obesity-associated inflammasome activation in adipose tissue, which was shown to be unaffected by $P2X_7R$ ablation (Sun et al. 2012). This latter finding is consistent with our results that metabolic parameters were worsened to a similar extent in WT and $P2X7R^{-/-}$ mice on a HFD. This is also in keeping with the concept that regulation of inflammasome activation is tissue-specific. On the other side, the observation that post-translational processing of pro-caspase-1, a marker of inflammasome activation (Yazdi et al. 2010), as well as renal inflammation and injury were not completely suppressed in $P2X_7R^{-/-}$ mice suggests that other inflammasomes and/or non-inflammasome pro-inflammatory pathways participate in HFD-induced renal disease.

Three, not mutually exclusive models have been proposed for inflammasome activation (Schroder and Tschopp 2010): pore formation, induced by eATP via $P2X_7R$ or by pore-forming toxins, which triggers K^+ efflux and allows extracellular NLRP3 agonists to access the cytosol; frustrated phagocytosis of crystalline and particulate structures, with consequent lysosomal disintegration and release of proteases; and ROS generation via NADPH oxidase or mitochondrial sources, which may represent a common final pathway. All three models might be involved in the activation of the NLRP3 inflammasome in HFD-fed mice, via multiple signals including saturated FFAs such as palmitate (Wen et al. 2011), the product of long

chain saturated FFAs ceramide (Vandanmagsar et al. 2011), modified lipoproteins such as oxidized LDLs, via formation of cholesterol crystals (Duewell et al. 2010), glucose, ROS, and eATP and uric acid released by dead cells (Strowig et al. 2012). The finding that activation of the NLRP3 inflammasome was blunted by $P2X_7R$ ablation implies that $P2X_7R$ plays a central role in this phenomenon and suggests that FFAs and glucose, by up-regulating $P2X_7R$ (Glas et al. 2009), as well as eATP, by engaging $P2X_7R$ (Ward et al. 2010), are likely involved in NLRP3 activation under these conditions.

An important observation of our study is that not only the activation of the NLRP3 inflammasome, but also the activation of the NF-kB and, consequently, the transcription of the inflammasome components and targets were reduced by $P2X_7R$ ablation. As known, the generation of mature IL-1β and IL-18 involves two separate processes to avoid their inappropriate and deleterious release: the induction of NF-kB-dependent mRNA expression and translation of the procytokine upon activation by most PRRs (signal 1) followed by cleavage of the procytokine and release of its mature and active form via NLRP3 inflammasome activation (signal 2). It is plausible that the strong reduction of the NF-kB activation in $P2X_7R^{-/-}$ mice fed HFD vs. WT can result from a damping in $P2X_7R$-deficient mice of the auto-activating positive loop, by which mature inflammatory cytokines, including IL1β and IL18, binding to their membrane receptor, trigger the NF-kB activation stimulating the overexpression of themselves (Bonizzi and Karin 2004). On the other hand, the demonstration by Liu and colleagues that $P2X_7R$ is involved in the activation of NF-kB, mediated probably by a direct interaction with LPS and ATP (Liu et al. 2011), in addition to the evidence that biglycan, an ECM component released during ECM remodeling, was shown to mediate the interaction of TLR2/4 with $P2X_7R$ /$P2X_4R$, thus leading to both priming and activation of the NLRP3 inflammasome (Babelova et al. 2009), suggests that in our model this receptor can play also a direct role in NF-kB activation, so acting not only as signal 2 but also as signal 1 in the NLRP3 inflammasome activation.

Moreover, although no differences in kidney lipid accumulation between the two genotype were present, $P2X_7R^{-/-}$ mice fed HFD vs. WT showed lower oxidative and carbonyl stress. This is consistent with the reduced protein expression of the renal isoform of NADPH oxidase, NOX 4, associated with the ablation of $P2X_7R$. These data are supported by the recent demonstration that $P2X_7R$ is a mediator of oxidative

stress via NADPH oxidase both in vivo (Chatterjee et al. 2012) and in vitro (Liu et al. 2011, Korcok et al. 2004) and corroborate a role for this receptor as a source of ROS signals for priming and possibly activation of the NLRP3 inflammasome.

Finally, data from human kidneys support a role for the $P2X_7R$ -NLRP3 axis also in renal disease associated with type 2 diabetes and metabolic disorders, consistent with a previous report that NLRP3 mRNA expression was increased in human renal biopsies from subjects with non-diabetic CKD (Vilaysane et al. 2010). A causal role for the NLRP3 inflammasome has been recently suggested by the observations that IL-1 receptor antagonist gene polymorphism affects CKD progression, especially in subjects with diabetic nephropathy (Buraczynska et al. 2006), and that a human-engineered monoclonal anti-IL-1β antibody reduces inflammation in patients with type 2 diabetes (Cavelti-Weder et al. 2012).

5.2 Liver disease. Non-alcoholic fatty liver disease (NAFLD) is one of the major complications of the insulin resistance and MS (Marchesini et al. 2003), that encompasses various pathologic conditions, from simple steatosis to nonalcoholic steato-hepatitis (NASH), cirrhosis, and possibly hepatocellular carcinoma (Erickson 2009). Fat accumulates within the liver via increased fatty acid (FA) delivery from adipose tissue and diet and enhanced hepatic FA import and synthesis exceeding the rate of FA export and catabolism (Bradbury and Berk 2004)

To date, the involvement of $P2X_7R$ in the pathophysiology of liver disease is largely unknown and restricted to model of acute hepatic injury induced by toxic substances (Hoque et al. 2012, Chatterjee et al. 2012.). Here, we provide the first evidence that $P2X_7R$ ablation influences the earlier steps of NAFLD, i.e. steatosis, hepatocyte injury, and inflammation, since $P2X_7R$-deficient mice showed marked attenuation or even prevention of NASH induced by a high fat diet. NASH prevention/attenuation was attested by reduced infiltration of inflammatory cells, blunted up-regulation of proinflammatory cytokines and transcription factor and decreased fibrosis.

Hepatic fat accumulation was also lower in the liver of $P2X_7R^{-/-}$ than in WT mice fed the HFD, despite similar increases in circulating lipids and the same extent of

insulin resistance (IR). This may be attributed to the improved hepatic lipid metabolism showed by the transgenic mice, resulting from the lower transcriptional levels of genes implicated in the lipogenesis process and a more favorable modulation of genes involved in the regulation of cholesterol and fatty acid homeostasis. So, we can speculate that $P2X_7R$ ablation protects mice from the onset of early pro-inflammatory changes induced by increase of fatty acids delivery from adipose tissue and diet, thus limiting hepatocytes injury and, consequently, their lipid metabolism impairment. This series of events, in turn, causes a lower fat accumulation, i.e. steatosis, and, over time, less inflammation characteristic of NASH in $P2X_7R^{-/-}$ mice fed HFD vs. WT.

To date, the mechanism through which the $P2X_7R$ exerts its pro-inflammatory role in HFD-induced NAFLD is unknown. However, the strong NLRP3 positive staining of some liver structures (i.e., hepatic sinusoids, bile duct epithelial cells) and infiltrating inflammatory cells observed in WT mice fed HFD, but not in $P2X7R^{-/-}$ HFD animals, suggests that in the liver, as well as in the kidney, $P2X_7R$ may act as an NLRP3 inflammasome modulator/activator. Consistently with this hypothesis, Csak and colleagues recently showed an implication of the NLRP3 inflammasome in the pathogenesis of NASH induced by methionine choline-deficient (MCD) or long-term high fat diet, proving that the saturated fatty acid (FA) palmitic acid (PA) activates the inflammasome in the liver and induces sensitization to lipopolysaccharide (LPS)-induced IL1β release in hepatocytes. Furthermore, hepatocytes exposed to saturated FAs release danger signals that trigger inflammasome activation in immune cells (Csak et al. 2011). However, more work is needed to confirm this speculation.

Conclusion. In conclusion, these data demonstrate a major contribution of the $P2X_7R$ in the process driving both renal and hepatic inflammation and injury associated with metabolic disorders. Moreover, at least in the kidney, $P2X_7R$ acts as both signal 1 and signal 2 in the induction and activation of the NLRP3 inflammasome. Thus, this study identifies $P2X_7R$ and NLRP3 as novel therapeutic targets for kidney and liver disease associated with metabolic disorders such as type 2 diabetes and the metabolic syndrome.

References

Agostini L. et al. NALP3 forms an IL-1beta-processing inflammasome with increased activity in Muckle-Wells autoinflammatory disorder. Immunity. 2004;20(3):319-25.

Anders HJ and Muruve DA. The inflammasomes in kidney disease. J Am Soc Nephrol 2011; 22: 1007-1018.

Babelova A. et al. Biglycan, a danger signal that activates the NLRP3 inflammasome via toll-like and P2X receptors. J Biol Chem 2009; 284: 24035-24048.

Bauernfeind F. et al. Inflammasomes: current understanding and open questions. Cell Mol Life Sci. 2011;68(5):765-83.

Bauernfeind FG. et al.Cutting edge: NF-kappaB activating pattern recognition and cytokine receptors license NLRP3 inflammasome activation by regulating NLRP3 expression. J Immunol. 2009 15;183(2):787-91.

Beigi R. et al. Detection of local ATP release from activated platelets using cell surface-attached firefly luciferase. Am J Physiol. 1999 Jan;276:C267-78.

Bonizzi G and Karin M. The two NF-kappaB activation pathways and their role in innate and adaptive immunity.Trends Immunol. 2004;25(6):280-8.

Bours MJ. Et al. P2 receptors and extracellular ATP: a novel homeostatic pathway in inflammation. Front Biosci (Schol Ed) 2011; 3: 1443-1456.

Bradbury MW and Berk PD. Lipid metabolism in hepatic steatosis. Clin Liver Dis 2004;8:639–671.

Buell G et al. Blockade of human P2X7 receptor function with a monoclonal antibody. Blood 1998; 92; 3521 – 28.

Buraczynska M et al. Interleukin-1 receptor antagonist gene polymorphism affects the progression of chronic renal failure. Cytokine 2006; 36: 167-172.

Burnstock G. Physiology and pathophysiology of purinergic neurotransmission. Physiol Rev. 2007;87(2):659-797.

Burnstock G and Knight GE. Cellular distribution and functions of P2 receptor subtypes in different systems. Int Rev Cytol 2004;240: 31 – 304.

Castelli WP. et al. Incidence of coronary heart disease and lipoprotein cholesterol levels. The Framingham Study. JAMA 1986; 256: 2835-2838.

Cavelti-Weder C. et al. Effects of Gevokizumab on glycemia and inflammatory markers in type 2 diabetes. Diabetes Care 2012; 35: 1654-1662.

Chatterjee S et al. P2X7 receptor-NADPH oxidase axis mediates protein radical formation and Kupffer cell activation in carbon tetrachloride-mediated steatohepatitis in obese mice. Free Radic Biol Med. 2012;52(9):1666-79.

Coddou C et al. Activation and regulation of purinergic P2X receptor channels. Pharmacol Rev. 2011;63(3):641-83.

Cook GP. et al. The NLRP3 inflammasome, a target for therapy in diverse disease states. Eur J Immunol. 2010;40(3):631-4.

Csak T et al. Fatty acid and endotoxin activate inflammasomes in mouse hepatocytes that release danger signals to stimulate immune cells. Hepatology. 2011;54(1):133-44.

Deji N. et al. Structural and functional changes in the kidneys of high-fat diet-induced obese mice. Am J Physiol Renal Physiol 2009; 296: F118-F126.

Denlinger LC et al. Cutting edge: the nucleotide receptor P2X7 contains multiple protein- and lipid-interaction motifs including a potential binding site for bacterial lipopolysaccharide. J Immunol. 2001 Aug 15;167(4):1871-6.

De Nardo D. and Latz E. NLRP3 inflammasomes link inflammation and metabolic disease. Trends Immunol. 2011;32(8):373–9.

Donnelly-Roberts DL and Jarvis MF. Discovery of P2X7 receptor-selective antagonists offers new insights into P2X7 receptor function and indicates a role in chronic pain states. Br J Pharmacol 2007; 151: 571 – 79.

Dröge W. Free radicals in the physiological control of cell function. Physiol Rev. 2002;82(1):47-95.

Duewell P. et al. NLRP3 inflammasomes are required for atherogenesis and activated by cholesterol crystals. Nature. 2010 29;464(7293):1357-61

Eisenbarth SC. et al. Crucial role for the Nalp3 inflammasome in the immunostimulatory properties of aluminium adjuvants. Nature. 2008;453(7198):1122–6. 46.

Elliott JI, et al. Membrane phosphatidylserine distribution as a non-apoptotic signalling mechanism in lymphocytes. Nat Cell Biol 2005; 7: 808–816.

Erickson SK. Nonalcoholic fatty liver disease. J Lipid Res 2009;50:S412–416.

Febbraio M et al. Targeted disruption of the class B scavenger receptor CD36 protects against atherosclerotic lesion development in mice. J Clin Invest. 2000;105(8):1049-56.

Ferrari D. et al. The P2X7 receptor: a key player in IL-1 processing and release. J Immunol. 2006;176(7):3877-83.

Ferrari D. et al. Extracellular ATP triggers IL-1 beta release by activating the purinergic P2Z receptor of human macrophages. J. Immunol. 1997;159: 1451–1458.

Ferrari D. et al. Extracellular ATP activates transcription factor NF-kappaB through the P2Z purinoreceptor by selectively targeting NF-kappaB p65. J Cell Biol. 1997;139(7):1635-43.

Ferrari D. et al. Mouse microglial cells express a plasma membrane pore gated by extracellular ATP. J. Immunol. 1996; 156: 1531–1539.

Franchi L, Eigenbrod T and Núñez G. Cutting edge: TNF-alpha mediates sensitization to ATP and silica via the NLRP3 inflammasome in the absence of microbial stimulation. J Immunol. 2009 15;183(2):792-6.

Glas R et al. Purinergic P2X7 receptors regulate secretion of interleukin-1 receptor antagonist and beta cell function and survival. Diabetologia 2009; 52: 1579-1588.

Gombault A, Baron L and Couillin I. ATP release and purinergic signaling in NLRP3 inflammasome activation. Front Immunol. 2012;3:414.

Gonçalves RG et al. The role of purinergic P2X7 receptors in the inflammation and fibrosis of unilateral ureteral obstruction in mice. Kidney Int 2006; 70: 1599-1606.

Gorin Y. et al. Nox4 NAD(P)H oxidase mediates hypertrophy and fibronectin expression in the diabetic kidney. J Biol Chem. 2005;280(47):39616-26.

Griffiths, R. J.et al. ATP induces the release of IL-1 from LPS-primed cells in vivo. J. Immunol. 1995; 154: 2821–2828.

Gu BJ et al. An Arg307 to Gln polymorphism within the ATP-binding site causes loss of function of the human P2X7 receptor. J Biol Chem 2004; 279: 31287 – 95.

Gu BJ et al.Expression of P2X7 purinoceptors on human lymphocytes and monocytes: evidence for nonfunctional P2X7 receptors. Am J Phys Cell Phys 2000; 279: C1189 – 97.

Guarda G. et al. Differential expression of NLRP3 among hematopoietic cells. J Immunol. 2011;186(4): 2529–34.

Halle, A. et al. The NALP3 inflammasome is involved in the innate immune response to amyloid-beta. Nat. Immunol. 2008; 9, 857–865.

Harada H et al. Induction of proliferation and apoptotic cell death via P2Y and P2X receptors, respectively, in rat glomerular mesangial cells. Kidney Int. 2000;57(3):949-58.

Haskó G et al. Adenosine receptors: therapeutic aspects for inflammatory and immune diseases. Nat Rev Drug Discov. 2008;7(9):759-70.

Hibell AD et al. Complexities of measuring antagonist potency at P2X7 receptor orthologs. J Pharmacol Exp Ther 2001; 296: 947 – 57.

Hoque R et al. P2X7 receptor-mediated purinergic signaling promotes liver injury in acetaminophen hepatotoxicity in mice. Am J Physiol Gastrointest Liver Physiol. 2012; 302(10):G1171-9.

Hornung V. et al. Silica crystals and aluminum salts activate the NALP3 inflammasome through phagosomal destabilization. Nat. Immunol. 2008; 9, 847–856.

Hotamisligil G.S. Inflammation and metabolic disorders. Nature 2006; 444: 860-867

Humphreys BD et al. Isoquinolines as antagonists of the P2X7 nucleotide receptor: high selectivity for the human versus rat receptor homologues. Mol Pharmacol. 1998;54(1):22-32.

Iacobini C et al. Advanced lipoxidation end-products mediate lipid-induced glomerular injury: role of receptor-mediated mechanisms. J Pathol 2009; 218: 360-369.

Iacobini C. et al. Development of age-dependent glomerular lesions in galectin-3/AGE-receptor-3 knockout and wild type mice. Am J Physiol (Renal Physiol) 2005; 289: F611-F621

Jacobson KA and Gao ZG. Adenosine receptors as therapeutic targets. Nature Rev. Drug Discov 2006;5:247–264.

Jiang LH. Inhibition of P2X7 receptors by divalent cations: old action and new insight. Eur Biophys J 2009; 38: 339 – 46.55.

Jiang LH et al. Identification of amino acid residues contributing to the ATP-binding site of a purinergic P2X receptor. J Biol Chem. 2000; 3;275(44):34190-6.

Jiang T et al. Diet-induced obesity in C57BL/6J mice causes increased renal lipid accumulation and glomerulosclerosis via a sterol regulatory element-binding protein-1c-dependent pathway. J Biol Chem 2005; 280: 32317-32325.

Kawamura H et al. P2X7 receptors regulate NKT cells in autoimmune hepatitis. J Immunol. 2006;176(4):2152-60.

Kim M and al. Proteomic and functional evidence for a P2X7 receptor signalling complex.EMBO J. 2001; 15;20(22):6347-58.

Kahlenberg, J. M. and G. R. Dubyak. Mechanisms of caspase-1 activation by P2X7 receptor-mediated K release. Am. J. Physiol. 2004; 286: C1100 –C1108.

Kanneganti, T.D et al. Pannexin-1-mediated recognition of bacterial molecules activates the cryopyrin inflammasome independent of Toll-like receptor signaling. Immunity 2007; 26, 433–443.

Kassi E. et al. Metabolic syndrome: definitions and controversies. BMC Med. 2011 5;9:48.

Klinkner AM. et al. Evidence of foam cell and cholesterol crystal formation in macrophages incubated with oxidized LDL by fluorescence and electron microscopy. J. Histochem. Cytochem. 1995 43, 1071–1078

Korcok J. Extracellular nucleotides act through P2X7 receptors to activate NF-kappaB in osteoclasts. J Bone Miner Res. 2004; 19: 642-651.

Krane V and Wanner C. Statins, inflammation and kidney disease. Nat Rev Nephrol 2011;7: 385-397.

Kume S et al. Role of altered renal lipid metabolism in the development of renal injury induced by a high-fat diet. J Am Soc Nephrol 2007; 10: 2715-2723.

Kurella M, Lo JC and Chertow GM. Metabolic syndrome and the risk for chronic kidney disease among nondiabetic adults. J Am Soc Nephrol 2005; 16:2134-2140.

Lamkanfi, M. et al. Glyburide inhibits the cryopyrin/Nalp3 inflammasome. J.Cell Biol. 2009; 187, 61–70.

Labasi JM et al. Absence of the P2X7 receptor alters leukocyte function and attenuates an inflammatory response. J Immunol. 2002;168(12):6436-45.

Liu Y, Xiao Y, Li Z. P2X7 receptor positively regulates MyD88-dependent NF-kB activation. Cytokine. 2011;55(2):229-36.

MacKenzie A. et al. Rapid secretion of interleukin-1beta by microvesicle shedding. Immunity. 2001; 15:825–35.

Maedler, K. et al. Glucose-induced beta cell production of IL-1β contributes to glucotoxicity in human pancreatic islets. J. Clin. invest. 2002; 110, 851–860. 53.

Majno G and Joris I. Apoptosis, oncosis, and necrosis. An overview of cell death. Am J Pathol. 1995;146(1):3-15.

Mandrup-Poulsen, T., Pickersgill, L. and Donath, M.Y. Blockade of interleukin 1 in type 1 diabetes mellitus. nat. Rev. endocrinol. 2010; 6, 158–166.

Marchesini G et al. Nonalcoholic fatty liver, steatohepatitis, and the metabolic syndrome. Hepatology 2003;37:917–923

Mariathasan S. et al. Cryopyrin activates the inflammasome in response to toxins and ATP. Nature. 2006;440(7081):228-32.

Martinon F. Signaling by ROS drives inflammasome activation. Eur J Immunol. 2010;40(3):616-9.

Martinon F, Mayor A and Tschopp J. The inflammasomes: guardians of the body. Annu Rev Immunol. 2009;27:229-65

Martinon F. Detection of immune danger signals by NALP3. J Leukoc Biol. 2008;83(3):507-11.

Martinon F et al. Gout- associated uric acid crystals activate the NALP3 inflammasome. Nature. 2006;440(7081):237–41.

Masters, S.L. et al. Activation of the NLRP3 inflammasome by islet amyloid polypeptide provides a mechanism for enhanced IL-1β in type 2 diabetes. nat. immunol. 2010;11, 897–904.

McCall SH. et al. Osteoblasts express NLRP3, a nucleotide-binding domain and leucine-rich repeat region containing receptor implicated in bacterially induced cell death. J. Bone Miner. Res. 2008;23:30–40

Miao EA, Rajan JV and Aderem A. Caspase-1-induced pyroptotic cell death. Immunol Rev. 2011;243(1):206-14

Neuschwander-Tetri BA and Caldwell SH. Nonalcoholic steatohepatitis: summary of an AASLD Single Topic Conference. Hepatology. 2003;37(5):1202-19.

Niemi K,. et al. Serum amyloid A activates the NLRP3 inflammasome via P2X7 receptor and a cathepsin B-sensitive pathway. J Immunol. 2011;186(11):6119–28.

North RA. Molecular physiology of P2X receptors. Physiol Rev. 2002;82(4):1013-67.

Novak I. Purinergic receptors in the endocrine and exocrine pancreas. Purinergic Signal 2008: 4: 237 – 53.

Novak I. ATP as a signaling molecule: the exocrine focus. News Physiol Sci. 2003;18:12-7.

Pelegrin P and Surprenant A. The P2X(7) receptor-pannexin connection to dye uptake and IL-1beta release. Purinergic Signal. 2009;5(2):129-37.

Pelegrin P and Surprenant A. Pannexin-1 mediates large pore formation and interleukin-1beta release by the ATP-gated P2X7 receptor. EMBO J. 2006 1;25(21):5071-82.

Pellegatti P. et al. A novel recombinant plasma membrane-targeted luciferase reveals a new pathway for ATP secretion. Mol Biol Cell 2005; 16:3659-65

Perregaux, D. and C. A. Gabel. Interleukin-1 beta maturation and release in response to ATP and nigericin: evidence that potassium depletion mediated by these agents is a necessary and common feature of their activity. J. Biol. Chem. 1994; 269: 15195–15203.

Qu Y et al. Nonclassical IL-1 beta secretion stimulated by P2X7 receptors is dependent on inflammasome activation and correlated with exosome release in murine macrophages. J Immunol. 2007;179(3):1913-25.

Ralevic V. and Burnstock G. Receptors for Purines and Pyrimidines. Pharmacol Rev 1998; 50: 413-492

Riteau N et al. ATP release and purinergic signaling: a common pathway for particle-mediated inflammasome activation. Cell Death Dis 2012; 11;3

Salminen A. et al. Amyloid-beta oligomers set fire to inflammasomes and induce Alzheimer's pathology. J Cell Mol Med. 2008;12(6A):2255–62.

Sanz, J. M. and F. Di Virgilio. Kinetics and mechanism of ATP-dependent IL-1 release from microglial cells. J. Immunol. 2000;164: 4893– 4898.

Schroder K and Tschopp J. The inflammasomes. Cell. 2010 19;140(6):821-32

Schwiebert E. M. ATP release mechanism, ATP receptors and purinergic signaling along the nephron. Clinical and Experimental Pharmacology and Physiology 2001; 28, 340–350

Sluyter, R., A. N. Shemon and J. S. Wiley. Glu496 to Ala polymorphism in the P2X7 receptor impairs ATP-induced IL-1 release from human monocytes. J. Immunol. 2004;172: 3399 –3405.

Smart ML et al. P2X7 receptor cell surface expression and cytolytic pore formation are regulated by a distal C-terminal region. J Biol Chem. 2003;7;278(10):8853-60.

Solini A et al. Multiple P2X receptors are involved in the modulation of apoptosis in human mesangial cells: evidence for a role of P2X4. Am J Physiol Renal Physiol. 2007;292(5):F1537-47.

Solini A et al. Purinergic modulation of mesangial extracellular matrix production: role in diabetic and other glomerular diseases. Kidney Int. 2005;67(3):875-85.

Solini A et al. Human primary fibroblasts in vitro express a purinergic P2X7 receptor coupled to ion fluxes, microvesicle formation and IL-6 release. J Cell Sci 1999; 112: 297 – 305.

Solle M. et al. Altered cytokine production in mice lacking P2X7 receptors. J. Biol. Chem. 2001; 276: 125–132.

Stewart CR et al. CD36 ligands promote sterile inflammation through assembly of a Toll-like receptor 4 and 6 heterodimer. Nat Immunol. 2010;11(2):155-61.

Stienstra, R. et al. Inflammasome is a central player in the induction of obesity and insulin resistance. Proc. natl. acad. sci. Usa 2011;108, 15324–15329.

Stienstra, R. et al. The inflammasome-mediated caspase-1 activation controls adipocyte differentiation and insulin sensitivity. Cell metab. 2010;12, 593–605.

Strowig T et al. Inflammasomes in health and disease. Nature 2012; 280: 278-286.

Sun S et al. The ATP-P2X7 signaling axis is dispensable for obesity-associated inflammasome activation in adipose tissue. Diabetes 2012; 61: 1471-1478.

Sun L et al. Role of sterol regulatory element-binding rotein 1 in regulation of renal lipid metabolism and glomerulosclerosis in diabetes mellitus. J Biol Chem 2002; 277: 18919-18927.

Surprenant A and North RA. Signaling at purinergic P2X receptors. Annu Rev Physiol. 2009;71:333-59.

Surprenant A. et al. The cytolytic P2Z receptor for extracellular ATP identified as a P2X receptor (P2X7). Science 1996; 272: 735-738

Taylor SR et al. P2X7 deficiency attenuates renal injury in experimental glomerulonephritis. J Am Soc Nephrol 2009; 20: 1275-1281.

Ting JP et al. The NLR gene family: a standard nomenclature. Immunity 2008; 28:285–287

Turner CM et al. Increased expression of the pro-apoptotic ATP-sensitive P2X7 receptor in experimental and human glomerulonephritis.Nephrol Dial Transplant. 2007;22(2):386-95.

Valko M et al. Free radicals and antioxidants in normal physiological functions and human disease. Int J Biochem Cell Biol. 2007;39(1):44-84.

Vandanmagsar B. et al. The NLRP3 inflammasome instigates obesity-induced inflammation and insulin resistance. Nat Med. 2011;17(2):179-88.

Vilaysane A. et al. The NLRP3 inflammasome promotes renal inflammation and contributes to CKD. J Am Soc Nephrol 2010; 21: 1732-1744.

Vonend O et al. Glomerular expression of the ATP-sensitive P2X receptor in diabetic and hypertensive rat models. Kidney Int. 2004;66(1):157-66.

Ward JR et al. Temporal interleukin-1beta secretion from primary human peripheral blood monocytes by P2X7-independent and P2X7-dependent mechanisms. J Biol Chem 2010; 285: 23147-23158.

Wen H et al. A role for the NLRP3 inflammasome in metabolic diseases—did Warburg miss inflammation? Nat. Immunol 2012; 13: 352-357.

Wen H et al. Fatty acid-induced NLRP3-ASC inflammasome activation interferes with insulin signaling. Nat Immunol. 2011;12(5):408-15

Westermark, P., Andersson, A., and Westermark, G.T. Islet amyloid polypeptide, islet amyloid, and diabetes mellitus. Physiol. Rev. 2011; 91, 795–826.

Wiley JS et al. The human P2X7 receptor and its role in innate immunity. Tissue Antigens. 2011;78(5):321-32.

Wilson HL et al. P2X receptor characterization and IL-1/IL-1Ra release from human endothelial cells. Br J Pharmacol 2007; 151:115 – 127.

Yan Z et al. Experimental characterization and mathematical modeling of P2X7 receptor channel gating. J Neurosci. 2010;30(42):14213-24.

Yan Z et al. The P2X7 receptor channel pore dilates under physiological ion conditions. J Gen Physiol. 2008; Nov;132(5):563-73.

Yazdi AS et al. Inflammatory caspases in innate immunity and inflammation. J Innate Immun 2010; 2: 228-237.

Zambetti LP et al. The rhapsody of NLRPs: master players of inflammation...and a lot more. Immunol Res. 2012;53(1-3):78-90.

Zhou, R et al. Thioredoxin-interacting protein links oxidative stress to inflammasome activation. nat. immunol. 2010;11, 136–140.